Catalysis Today 151 (2010) 395–409

Contents lists available at ScienceDirect

Catalysis Today

journal homepage: www.elsevier.com/locate/cattod

Modelling of a combined NO_x storage and NH_3-SCR catalytic system for Diesel exhaust gas aftertreatment

Daniel Chatterjee [a,*], Petr Kočí [b], Volker Schmeißer [a], Miloš Marek [b], Michel Weibel [a], Bernd Krutzsch [a]

[a] Daimler AG, Department GR/APE-Combustion and Emission Control, 019-G206, D-70 546 Stuttgart, Germany
[b] Institute of Chemical Technology, Prague, Department of Chemical Engineering, Technická 5, CZ-166 28 Praha, Czech Republic

ARTICLE INFO

Article history:
Available online 8 April 2010

Keywords:
NO_x storage catalyst
Lean NO_x trap
Selective NO_x reduction
NH_3
Mathematical modelling
Automobile exhaust gas conversion

ABSTRACT

A combined Diesel exhaust gas aftertreatment system is studied, consisting of the NO_x storage and reduction catalyst (NSRC, called also lean NO_x trap, LNT) and the catalyst for selective catalytic reduction of NO_x by NH_3 (NH_3-SCR). Most of the time the system is operated under prevailing fuel-lean conditions, enabling economical running of the engine. During this phase the NO_x emissions are being adsorbed in the NSRC. However, short fuel enrichments need to be applied periodically for the NSRC regeneration (reduction of the stored NO_x). Ammonia produced in the NSRC as a by-product of the NO_x reduction under controlled fuel-rich conditions is then adsorbed in the NH_3-SCR reactor located downstream. The adsorbed NH_3 is consequently utilised in selective NO_x reduction during the next fuel-lean period. The NSRC + SCR configuration thus eliminates the need for an external NH_3 source (e.g., periodically re-filled urea solution tank) that is necessary in the case of the stand-alone SCR.

Development of effective mathematical models for the NSRC and SCR catalysts is discussed. Dynamic measurements in a lab mini-reactor are performed separately for the industrial NSRC (PtRh/Ba/Ce/γ-Al_2O_3 type) and SCR (Fe-ZSM type) catalyst samples. The experimental results are employed in the evaluation of rate parameters for the individual catalysts. Particular attention is given to the dynamic evolution of NH_3 during the NSRC regeneration and its dependence on temperature and length of the enrichment period. Trends in NH_3 selectivity with the NSRC ageing are discussed. Synergistic effects of the NSRC and NH_3-SCR are then studied by simulations of defined lean/rich operation and engine test driving cycles. The combined NSRC + SCR system provides higher NO_x conversions in comparison with the stand-alone NSRC and it prevents undesired NH_3 slip. The positive effects of the downstream SCR are most important at lower intermediate temperatures, and in the case of an aged NSRC that usually produces more NH_3.

1. Introduction

Burning lean fuel mixtures with excess of air brings a benefit in the form of lower fuel consumption. However, abatement of the NO_x emissions from Diesel and gasoline lean-burn engines is a complicated task because direct NO_x reduction is hindered under the oxidising conditions in the exhaust gas (in contrast to classical gasoline engines with stoichiometric fuel/air ratio leading to nearly neutral redox conditions). Even if the raw engine NO_x emissions are lowered by advanced combustion techniques and exhaust gas recirculation (EGR), exhaust gas aftertreatment in special deNO_x catalytic converters is necessary to meet the most strict emission limits [1,2]. Two technologies for the elimination of the NO_x emissions from lean-burn engines are nowadays used commercially in the automotive industry: NO_x storage and reduction catalyst (NSRC), and selective catalytic reduction of NO_x by NH_3 generated from a urea solution stored in a special tank (NH_3-SCR, urea-SCR).

The selective catalytic reduction of NO_x by NH_3 (SCR) was originally developed for stationary emission sources, mainly power plants [3]. However, it soon turned out to be a promising technology for the deNO_x in automobile applications as well [4]. In 2005 it was introduced for commercial heavy-duty vehicles in Europe, and more recently also for passenger cars [5]. The NH_3-SCR converter needs an external source of the selective reducing agent (ammonia). In standard configurations, the vehicle is equipped with a special tank containing the urea solution (marketed under different names, e.g., AdBlue) that needs to be re-filled periodically [2]. The urea solution is injected in a controlled way into the exhaust line, where it is

Abbreviations: DOC, Diesel oxidation catalyst; DPF, Diesel particulate filter; EUDC, extra-urban driving cycle (part of the NEDC); EGR, exhaust gas recirculation; HC, hydrocarbons; HT, hydro-thermal (catalyst pre-treatment); NM, Noble metals; NEDC, New European driving cycle (including cold start); NO_x, nitrogen oxides NO and NO_2 (excluding N_2O); NSRC, NO_x storage and reduction catalyst; OS, oxygen storage; SCR, selective catalytic reduction of NO_x; SV, (gas hourly) space velocity (at STP), h^{-1}; STP, standard $T = 273.15$ K and $p = 101,325$ Pa; TRM, transient response measurement.

* Corresponding author.
E-mail addresses: daniel.chatterjee@mtu-online.com (D. Chatterjee), petr.koci@vscht.cz (P. Kočí), volker.schmeisser@daimler.com (V. Schmeißer).
URL: http://www.vscht.cz/monolith

0920-5861/$ – see front matter © 2010 Elsevier B.V. All rights reserved.
doi:10.1016/j.cattod.2010.01.014

Latin letters

A_{NM}	noble metals activity (relative)
a	density of external surface area in monolith ($m^2\,m^{-3}$)
c_k	component concentration in bulk gas ($mol\,m^{-3}$)
c_k^s	component concentration in washcoat pores ($mol\,m^{-3}$)
c_p^g	specific heat capacity of gas ($J\,kg^{-1}\,K^{-1}$)
c_p^s	effective specific heat capacity of solid phase ($J\,kg^{-1}\,K^{-1}$)
d_h	inner equivalent diameter of the channel (m)
E_a	activation energy of reaction ($J\,mol^{-1}$)
J	number of reactions
k	reaction rate coefficient
k_0	pre-exponential constant of rate coefficient
k_c	mass transfer coefficient ($m\,s^{-1}$)
k_h	heat transfer coefficient ($J\,m^{-2}\,K^{-1}\,s^{-1}$)
K	number of gas components
K_a	inhibition coefficient
K_{LH}	equilibrium spill-over coefficient in SCR
K^{eq}	thermodynamic equilibrium constant, 1
L	length of monolith reactor (m)
M	number of surface-deposited components
r	transverse coordinate in catalytic washcoat layer (m)
R	reaction rate, $mol\,m^{-3}\,s^{-1}$ (related to washcoat volume)
R^g	universal gas constant, 8.31434 ($J\,mol^{-1}\,K^{-1}$)
t	time (s)
T	gas temperature (K)
T^s	temperature of solid phase (K)
T^e	temperature of surroundings (K)
v	linear gas velocity ($m\,s^{-1}$)
y_k	component mole fraction in bulk gas, 1
y_k^s	component mole fraction in washcoat pores, 1
Y	yield of selected product, 1
z	spatial coordinate along the monolith reactor (m)

Greek letters

β	reaction rate order with respect to selected component
γ	coefficient of coverage-dependent activation energy
δ	thickness of the washcoat layer (m)
ΔH_r	standard reaction enthalpy ($J\,mol^{-1}$)
ε^g	fraction of open frontal area in monolith, 1
ε^s	porosity of washcoat, 1
φ^s	volume fraction of active washcoat in entire solid phase, 1
λ^s	effective heat conductivity of solid phase, ($W\,m^{-1}\,K^{-1}$)
ν	stoichiometric coefficient, 1
θ	coverage of acidic non-reducible sites in SCR, 1
ρ^g	gas density ($kg\,m^{-3}$)
ρ^s	effective density of solid phase (incl. pores) ($kg\,m^{-3}$)
σ	coverage of redox sites in SCR, 1
τ	time interval (s)
ψ_m	coverage of the stored component, 1
ψ_m^{eq}	temperature-dependent saturation (equilibrium) coverage, 1
$\Psi_{cap,m}$	storage capacity, concentration of active sites ($mol\,m^{-3}$) (washcoat)
Ω	effective heat loss coefficient ($J\,m^{-3}\,K^{-1}\,s^{-1}$)

Subscripts and superscripts

eq	equilibrium
exp	experiment
in	inlet
j	index of reaction
k	index of gas component
m	index of stored (surface) component
out	outlet
s	solid phase (washcoat and monolith substrate)
sim	simulation

thermally decomposed into NH_3 and CO_2 [6]. The ammonia then reacts selectively with NO_x under lean (oxidising) conditions, giving N_2 as the final product. Different types of catalysts, mainly $V_2O_5/WO_3/TiO_2$ or zeolite formulations (Fe-ZSM5 and Cu-ZSM5) are currently used in the automotive industry.

The NO_x storage and reduction catalyst has been derived from classical three-way catalysts by adding NO_x adsorbing components into the active washcoat layer [7–9] (first implemented by Toyota with lean-burn gasoline engines). Typical formulation of the NSRC catalyst is NM/EA/OS/γ-Al_2O_3; here NM denotes noble metals (Pt,Rh,Pd), EA means earth alkaline or alkali metals serving as active components for the NO_x chemisorption [10,11], and OS are oxygen storage compounds (typically Ce oxides). The NSRC needs to be operated with periodic regenerations, i.e., temporarily increased concentration of the reducing components normally present in the exhaust gas (CO, H_2 and HC). In the course of a longer lean phase (economical engine operation with lean fuel mixture leading to oxidising conditions, lasting several minutes) the NO_x are adsorbed on the catalyst surface. The accumulated NO_x then need to be reduced within a controlled short rich phase (enrichment of fuel mixture leading to reducing conditions, lasting several seconds) [1,2]. As the NSRC contains noble metals, it possesses also the functionality of oxidation catalyst (DOC) or three-way catalyst (TWC) for CO and HC oxidation. The NSRC catalysts are primarily being used in passenger cars, while the SCR is well established for heavy-duty vehicles [12].

At the early stages of NSRC research it was not much reflected in the open literature (cf., e.g., review [11]) that besides the N_2, the desired main product of the NO_x reduction, also significant amounts of NH_3 can be formed depending on the regeneration phase length, temperature and gas composition. In the stand-alone NSRC, the regenerations need to be properly calibrated with respect to actual catalyst conditions (amount of NO_x stored, temperature, etc.) to avoid excessive NH_3 formation.

However, there exists a possibility to combine the ammonia generation in the NSRC with the ammonia utilisation in the SCR, cf. Fig. 1. The NSRC + SCR concept had been developed since late 1990s [13,14] and this system was launched into series production in 2006 with Mercedes E320 CDI BlueTec I [15,2]. Recently several integrated designs with multiple washcoat layers and/or multi-functional catalysts using the NSRC/SCR principle have been proposed, e.g., [16,17].

In this paper we present mathematical models for the NSRC + SCR system consisting of the two catalytic converters in series (Fig. 1). The independently developed NSRC and SCR models use

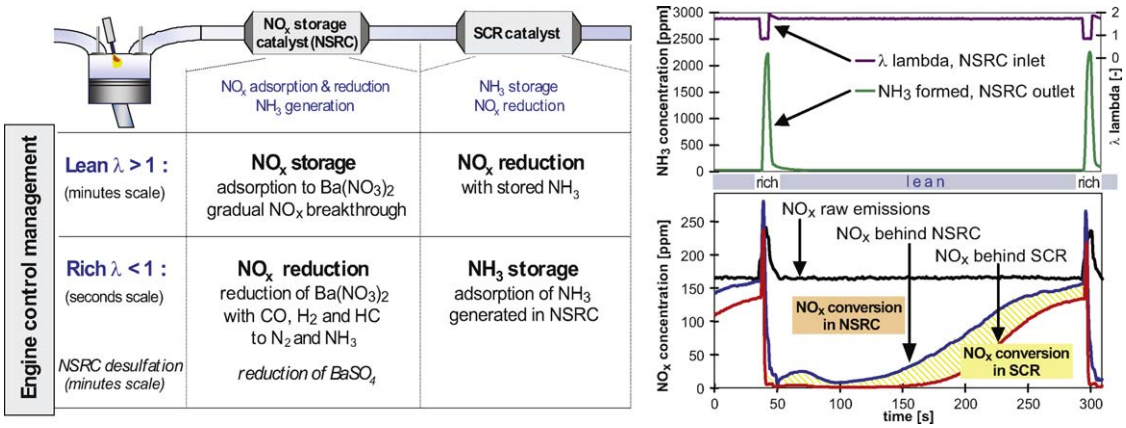

Fig. 1. Principle of the combined exhaust gas aftertreatment system consisting of NO_x storage & reduction catalyst (NSRC) and selective catalytic reduction of NO_x by NH_3 (SCR).

global reaction kinetics, calibrated on the basis of lab experiments with individual catalyst samples, and validated by engine test driving cycle data. The dynamic NSRC model developed in our prior work [18] for a de-greened catalyst is newly calibrated for a catalyst aged on road, and the resulting changes of effective NO_x storage capacity, NO_x conversion and NH_3 selectivity are discussed. The SCR model is derived from several studies devoted to particular reaction mechanisms in various NH_3-SCR systems [19–22]. It includes a non-equilibrium ammonia spill-over between the reactive and non-reactive sites that affects dynamic operation of the Fe-ZSM5 catalyst considered in this study. The models are then used for simulation and analysis of the NSRC + SCR system operation under varying conditions.

2. Mathematical model of catalytic monolith

A standard, spatially 2D(1D + 1D) heterogeneous model of a catalytic monolith channel with plug-flow and surface deposition of components is employed in the simulations, cf. e.g. [1]. The following balances are considered: mass balances in the flowing gas, including accumulation, convection, and external mass transfer (1); mass balances in the washcoat pores, including accumulation, internal diffusion, and catalytic reactions (2); mass balances on the catalyst surface, including accumulation, and catalytic reactions (3); enthalpy balance of the flowing gas, including accumulation, convection, and gas-solid heat transfer (4); enthalpy balance of the solid phase, including accumulation, axial heat conduction, gas-solid heat transfer, heat exchange with the surroundings, and heat source from catalytic reactions (5):

$$\frac{\partial c_k(z,t)}{\partial t} = -\frac{\partial(v\cdot c_k)}{\partial z} + \frac{k_c(z)a}{\varepsilon^g}\, c\,(y_k^s|_{r=\delta} - y_k), \quad k = 1,\ldots,K \tag{1}$$

$$\frac{\partial c_k^s(z,r,t)}{\partial t} = \frac{D_k^{\text{eff}}}{\varepsilon^s}\frac{\partial^2 c_k^s}{\partial r^2} + \frac{1}{\varepsilon^s}\sum_{j=1}^{J}\nu_{k,j}R_j, \quad k = 1,\ldots,K \tag{2}$$

$$\frac{\partial \psi_m(z,r,t)}{\partial t} = \frac{1}{\Psi_m^{\text{cap}}}\sum_{j=1}^{J}\nu_{m,j}^{\psi}R_j, \quad m = 1,\ldots,M \tag{3}$$

$$\rho c_p \frac{\partial T(z,t)}{\partial t} = -v\frac{\partial T}{\partial z}\rho c_p + \frac{k_h(z)a}{\varepsilon^g}(T^s - T) \tag{4}$$

$$\rho^s c_p^s \frac{\partial T^s(z,t)}{\partial t} = \lambda^s \frac{\partial^2 T^s}{\partial z^2} + \frac{k_h(z)a}{1-\varepsilon^g}(T - T^s) - \Omega(T^s - T^e) - \frac{a}{(1-\varepsilon^g)}\sum_{j=1}^{J}\int_{r=0}^{\delta}\Delta H_j R_j dr \tag{5}$$

The boundary conditions are in the form of Eqs. (6)–(10):

$$T|_{z=0} = T_{\text{in}}, \quad v|_{z=0} = v^{\text{in}} \tag{6}$$

$$\frac{\partial T^s}{\partial z}|_{z=0+} = 0, \quad \frac{\partial T^s}{\partial z}|_{z=L-} = 0 \tag{7}$$

$$c_k|_{z=0} = c_k^{\text{in}}, \quad k = 1,\ldots,K \tag{8}$$

$$D_k^{\text{eff}}\frac{\partial c_k^s}{\partial r}|_{r=\delta-} = k_c(z)c(y_k - y_k^s|_{r=\delta}), \quad k = 1,\ldots,K \ @\, r = \delta \tag{9}$$

$$\frac{\partial c_k^s}{\partial r}|_{r=0} = 0, \quad k = 1,\ldots,K \tag{10}$$

The axial coordinate $z = 0$ is located at the monolith inlet and $z = L$ corresponds to the monolith outlet. The transverse coordinate $r = \delta$ is at the top of the catalytic washcoat layer, while $r = 0$ corresponds to the bottom of the layer.

The reaction rates R_j employed in the NSRC and the SCR model will be discussed in detail in the next sections. If not explicitly stated, the local reaction rate coefficients k_j are calculated according to the Arrhenius dependence on temperature:

$$k_j = k_{j,0}\exp\left(\frac{-E_{a,j}}{R^g T^s}\right) \tag{11}$$

The inhibition coefficients K_{inh} are evaluated in a similar way. Different approaches regarding washcoat diffusion modeling have been used for the SCR and the NSRC simulation. To keep facile computation times for the more complex NSRC reaction system, a simplified balance of the catalytic washcoat layer (without explicit solution of internal diffusion) has been used. In this case transverse coordinate r was lumped, i.e., Eq. (2) was replaced by Eq. (12).

$$\frac{\partial c_k^s(z,t)}{\partial t} = \frac{k_c(z)a}{\varepsilon^s(1-\varepsilon^g)\varphi^s}c(y_k - y_k^s) + \frac{1}{\varepsilon^s}\sum_{j=1}^{J}\nu_{k,j}R_j, \quad k = 1,\ldots,K \tag{12}$$

In order to simulate combined exhaust aftertreatment systems, a modular and flexible software structure is required. A system simulation tool ExACT (Exhaust Gas Aftertreatment Components Toolbox) developed at Daimler [1,20,23] has been used to perform the simulations presented in this paper. Each catalytic monolith model together with the respective reaction kinetics and optimised numerical solver is written in Fortran and compiled into a respective library block. These library blocks can be arranged in sequence or in parallel exchanging all relevant information such as exhaust mass flow, temperature and species concentrations.

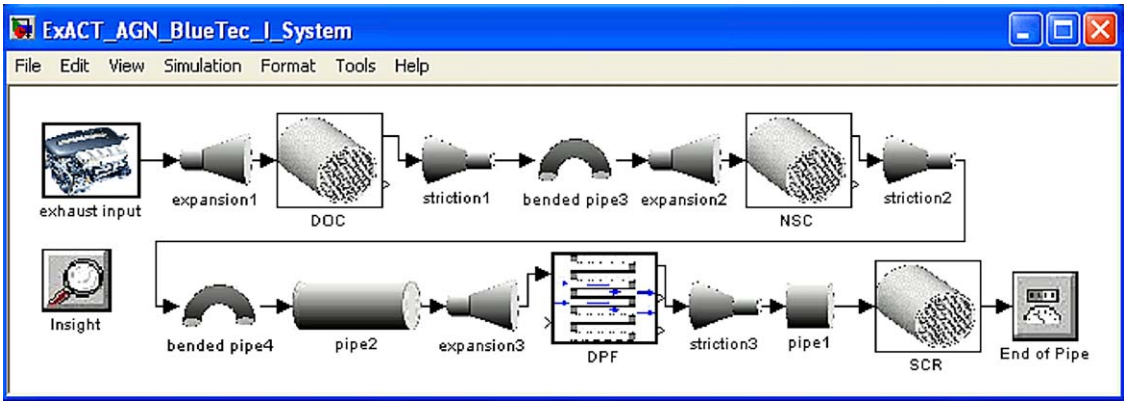

Fig. 2. Example of the ExACT simulation environment with a complex DOC + NSRC + DPF + SCR exhaust gas aftertreatment system.

ExACT also includes models for the connecting pipes, when the temperature loss between the individual aftertreatment components needs to be considered. An example of the ExACT environment is given in Fig. 2, where a complex exhaust gas aftertreatment system is shown, consisting of DOC, NSRC, DPF, and SCR.

In this paper we will focus on the NSRC + SCR subsystem specifically. The employed NSRC and SCR libraries were developed in co-operation with the Institute of Chemical Technology, Prague (NSRC), and Politecnico di Milano (SCR). They will be discussed in more detail in the next sections. Parameters of the studied NSRC and SCR monoliths are given in Table 1.

3. NO_x storage and reduction catalyst (NSRC)

Modelling of the NSRC reactions can be divided into two main parts – slow NO_x storage at the time scale of several minutes (lean phase), and fast transient reduction of the accumulated NO_x at the time scale of several seconds (rich phase), cf. Fig. 1. In both cases, the NSRC model has to be able to predict correctly not only NO_x but also CO and HC emissions, as well as NO_2/NO_x ratio in the outlet gas.

The combined NO_x adsorption mechanisms that occur during the lean phase have been investigated quite thoroughly since 1990s, including different types of NO_x storage sites present simultaneously in the washcoat, NO_2 disproportion, nitrites and nitrates, involvement of oxygen in the oxidation of the stored NO_x, contact between the noble metals and NO_x storage sites, and local diffusion effects — cf., e.g., the reviews [1,11].

More recently, details of dynamic NSRC regeneration and the role of the NO_x reduction intermediates and by-products have also been discussed in the open literature [24–33,18]. Transient reactions within the short rich phase involve interactions between the NO_x storage components, catalytic noble metals, and oxygen storage sites [26,28,32,18] and temperature waves caused by reaction exotherms [34].

Based on experimental observations and simulation studies [24–32,18], the NSRC regeneration dynamics and NH_3 evolution is generally interpreted in the following way: First an NO peak is observed at the outlet, resulting from the sudden desorption of weakly adsorbed NO_x without efficient reduction. The reducing front is travelling along the monolith channel from the inlet to the outlet, with an NH_3 concentration maximum on the moving boundary. Ammonia, formed mainly by the reaction of H_2 with NO_x under reducing conditions at the front part of the monolith, reacts with the NO_x and oxygen deposited on the unreduced catalyst surface at the rear part of the monolith, producing mainly N_2. Usually only smaller amounts of N_2O are formed as the product of incomplete NO_x reduction or NH_3 oxidation. The main NH_3 peak is observed in the exhaust gas when the reduction front reaches the reactor outlet. Correct description of the NSRC regeneration dynamics is possible only when local reaction kinetics is coupled with mass transport in the spatially distributed system of a catalytic monolith.

In a real exhaust gas mixture (CO, H_2, hydrocarbons, CO_2, H_2O), several other processes need to be considered in addition to the primary NH_3 source (i.e., the reaction of H_2 with NO_x). At higher temperatures ($T > 300\,^{\circ}C$), water gas shift and steam reforming take place in the NSRC under fuel-rich conditions, producing H_2 in situ from the present CO, HC and water [18]. Furthermore, NH_3 is formed also by the reaction of NO_x with CO in presence of water already at intermediate temperatures ($T \approx 200\,^{\circ}C$), well below the onset temperature for the water gas shift reaction [24,33,18]. This reaction proceeds most probably via formation and consequent hydrolysis of surface isocyanates [33].

Periodic lean/rich experiments at different temperatures have shown that the integral NO_x reduction selectivity to ammonia during the NSRC regeneration by hydrogen decreases with increasing temperature [28]. This is in agreement with observations that the NH_3 formation reaction with pure hydrogen (NO_x+H_2) takes place already at quite low temperatures, while the ammonia consumption (NH_3+NO_x) starts at somewhat higher

Table 1
Parameters of the used commercial NSRC and SCR monoliths (both catalysts coated on a cordierite substrate with square channels).

Parameter	NSRC	SCR
Catalyst type	PtRh/Ba/Ce/γ-Al_2O_3	Fe-ZSM5
Ageing state	Aged	De-greened
Ageing procedure	160 000 km on road	HT 5 h at 600 °C
Channels per cross-section area (cpsi)	400	300
Equivalent channel diameter (mm)	1.10	1.22
Wall thickness (μm)	110	170
Mean washcoat thickness δ (μm)	30	40
Open frontal area fraction ϵ^g (1)	0.750	0.688
Lab sample monolith diameter (cm)	2.54	Powder
Lab sample monolith length (cm)	1.52	Powder
Full-size monolith diameter (cm)	14.4	14.4
Full-size monolith length (cm)	19.7 / 9.85 [a]	19.7

[a] In simulations of driving cycle a half-size NSRC was used.

temperatures [30]. The speed of the reduction front varies with local NO_x and O_2 coverages and higher effective NO_x and O_2 storage capacities result in a longer delay before the main NH_3 peak appears at the reactor outlet [28].

However, in a realistic NO_x reduction mixture containing CO, H_2 and HC the activity of hydrogen at low temperatures is strongly inhibited, so that the maximum NH_3 yield is observed at intermediate temperatures, for a de-greened NSRC around 200–250 °C [18]. The effects of the rich gas composition during the regeneration phase are particularly important at lower intermediate temperatures when the NSRC regeneration is kinetically limited. At higher temperatures ($T > 350$ °C) the reduction of the stored NO_x is limited mainly by the feed of the reducing agents, and the NO_x conversions and NH_3 selectivities with CO, H_2 and HC become equivalent [18].

The reactions considered in the NSRC model are listed in Table 2. The model has been developed at the Institute of Chemical Technology, Prague [35] within the software package XMR designed for simulations of interconnected reactor-adsorber systems. The first version [36] was gradually extended by adding temperature-dependence of effective NO_x and oxygen storage capacity, NO/NO_2 transformation, water gas shift and steam reforming [34], detailed differentiation of CO, H_2 and HC activity [37], validation by real driving cycles [38], ammonia formation sub-model for the regeneration by H_2 [28], and finally a complete NSRC model involving dynamic ammonia generation and consumption within a realistic rich mixture (CO, H_2 and HC) where mutual inhibition effects were considered, again validated by real driving cycle data [18].

The first part of Table 2 (R_1^{NSRC}–R_{11}^{NSRC}) consists of global reactions taking place on noble metal sites (CO, H_2 and HC oxidation, water gas shift, steam reforming, NO_x reduction, reversible NO oxidation). These reactions are in principle common for all noble metal catalysts (TWC, DOC, NSRC). The reduction of

Table 2
Reactions on NO_x storage and reduction catalyst (NSRC), cf. [18]. Local mole fractions y^s in washcoat pores are considered in all reactions – the superscript "s" was omitted below for the sake of brevity.

Reaction step	Reaction rate
$CO + (1/2)O_2 \rightarrow CO_2$	$R_1^{NSRC} = k_1^{NSRC} A_{NM}\, y_{CO}\, y_{CO_2}/G_1$
$H_2 + (1/2)O_2 \rightarrow H_2O$	$R_2^{NSRC} = k_2^{NSRC} A_{NM}\, y_{H_2}\, y_{CO_2}/G_1$
$C_3H_6 + (9/2)O_2 \rightarrow 3CO_2 + 3H_2O$	$R_3^{NSRC} = k_3^{NSRC} A_{NM}\, y_{C_2H_6}\, y_{CO_2}/G_1$
$H_2O + CO \rightleftharpoons CO_2 + H_2$	$R_4^{NSRC} = k_4^{NSRC} A_{NM}\, [y_{CO}\, y_{H_2O} - y_{CO_2}\, y_{H_2}/K_{y,4}^{eq}]$
$3H_2O + C_3H_6 \rightarrow 3CO + 6H_2$	$R_5^{NSRC} = k_5^{NSRC} A_{NM} [y_{C_3H_6} y_{H_2O} - y_{CO}^3 y_{H_2}^6/(K_{y,5}^{eq} y_{H_2O}^2)]$
$NO + CO \rightarrow CO_2 + (1/2)N_2$	$R_6^{NSRC} = k_6^{NSRC} A_{NM}\, y_{CO}\, y_{NO}^{0.5}/G_1/G_2$
$NO + (5/2)H_2 \rightarrow H_2O + NH_3$	$R_7^{NSRC} = k_7^{NSRC} A_{NM}\, y_{H_2}\, y_{NO}^{0.5}/G_1/G_2$
$9NO + C_3H_6 \rightarrow 3CO_2 + 3H_2O + (9/2)N_2$	$R_8^{NSRC} = k_8^{NSRC} A_{NM}\, y_{C_2H_6}\, y_{NO}^{0.5}/G_1/G_2$
$NO + (1/2)O_2 \rightleftharpoons NO_2$	$R_9^{NSRC} = k_9^{NSRC} A_{NM}\, [y_{NO}\, y_{CO_2}^{0.5} - y_{NO_2}/K_{y,9}^{eq}]/G_1$
$NO_2 + CO \rightarrow NO + CO_2$	$R_{10}^{NSRC} = k_{10}^{NSRC} A_{NM}\, y_{NO_2}\, y_{CO}/G_6$
$9NO_2 + C_3H_6 \rightarrow 9NO + 3CO_2 + 3H_2O$	$R_{11}^{NSRC} = k_{11}^{NSRC} A_{NM}\, y_{NO_2}\, y_{C_2H_6}/G_6$
$Ce_2O_3 + (1/2)O_2 \rightarrow Ce_2O_4$	$R_{12}^{NSRC} = k_{12}^{NSRC}\, \Psi_{CO_2}^{cap}\, y_{CO_2}\, (\psi_{CO_2}^{eq} - \psi_{CO_2})$
$Ce_2O_4 + CO \rightarrow Ce_2O_3 + CO_2$	$R_{13}^{NSRC} = k_{13}^{NSRC}\, \Psi_{CO_2}^{cap}\, y_{CO}\, \psi_{CO_2}$
$Ce_2O_4 + H_2 \rightarrow Ce_2O_3 + H_2O$	$R_{14}^{NSRC} = k_{14}^{NSRC}\, \Psi_{CO_2}^{cap}\, y_{H_2}\, \psi_{CO_2}$
$Ce_2O_4 + (1/9)C_3H_6 \rightarrow Ce_2O_3 + (1/3)CO_2 + (1/3)H_2O$	$R_{15}^{NSRC} = k_{15}^{NSRC}\, \Psi_{CO_2}^{cap}\, y_{C_2H_6}\, \psi_{CO_2}$
$2NO_2 + (1/2)O_2 + BaO \rightarrow Ba(NO_3)_2$	$R_{16}^{NSRC} = k_{16}^{NSRC}\, \Psi_{NO_x}^{cap}\, y_{NO_2}\, (\psi_{NO_x}^{eq} - \psi_{NO_x})^2$ [a]
$2NO + (3/2)O_2 + BaO \rightleftharpoons Ba(NO_3)_2$	$R_{17}^{NSRC} = k_{17}^{NSRC}\, \Psi_{NO_x}^{cap}\, y_{NO}\, (\psi_{NO_x}^{eq} - \psi_{NO_x})^2$ [a]
$Ba(NO_3)_2 + 5CO \rightarrow N_2 + 5CO_2 + BaO$	$R_{18}^{NSRC} = k_{18}^{NSRC}\, \Psi_{NO_x}^{cap}\, y_{CO}\, \psi_{NO_x}^2/G_3$
$Ba(NO_3)_2 + 8CO + 3H_2O \rightarrow BaO + 8CO_2 + 2NH_3$	$R_{19}^{NSRC} = k_{19}^{NSRC}\, \Psi_{NO_x}^{cap}\, y_{CO}\, \psi_{NO_x}^2/G_3/G_5$
$Ba(NO_3)_2 + 8H_2 \rightarrow BaO + 5H_2O + 2NH_3$	$R_{20}^{NSRC} = k_{20}^{NSRC}\, \Psi_{NO_x}^{cap}\, y_{H_2}\, \psi_{NO_x}^2/G_3/G_5$
$Ba(NO_3)_2 + (5/9)C_3H_6 \rightarrow BaO + (5/3)CO_2 + (5/3)H_2O + N_2$	$R_{21}^{NSRC} = k_{21}^{NSRC}\, \Psi_{NO_x}^{cap}\, y_{C_2H_6}\, \psi_{NO_x}^2/G_3$
$Ba(NO_3)_2 + 3CO \rightarrow 2NO + 3CO_2 + BaO$	$R_{22}^{NSRC} = k_{22}^{NSRC}\, \Psi_{NO_x}^{cap}\, y_{CO}\, \psi_{NO_x}^2/G_4$
$Ba(NO_3)_2 + 3H_2 \rightarrow 2NO + 3H_2O + BaO$	$R_{23}^{NSRC} = k_{23}^{NSRC}\, \Psi_{NO_x}^{cap}\, y_{H_2}\, \psi_{NO_x}^2/G_4$
$Ba(NO_3)_2 + (1/3)C_3H_6 \rightarrow 2NO + CO_2 + H_2O + BaO$	$R_{24}^{NSRC} = k_{24}^{NSRC}\, \Psi_{NO_x}^{cap}\, y_{C_2H_6}\, \psi_{NO_x}^2/G_4$
$(10/3)NH_3 + Ba(NO_3)_2 \rightarrow BaO + 3H_2O + (8/3)N_2$	$R_{25}^{NSRC} = k_{25}^{NSRC}\, \Psi_{NO_x}^{cap}\, y_{NH_3}\, \psi_{NO_x}^2$
$2NH_3 + 3NO \rightarrow (5/2)N_2 + 3H_2O$	$R_{26}^{NSRC} = k_{26}^{NSRC} A_{NM}\, y_{NH_3}\, y_{NO}^{0.5}$
$2NH_3 + (3/2)O_2 \rightarrow N_2 + 3H_2O$	$R_{27}^{NSRC} = k_{27}^{NSRC} A_{NM}\, y_{NH_3}\, y_{CO_2}$
$2NH_3 + 3Ce_2O_4 \rightarrow N_2 + 3H_2O + 3Ce_2O_3$	$R_{28}^{NSRC} = k_{28}^{NSRC}\, \Psi_{CO_2}^{cap}\, y_{NH_3}\, \psi_{CO_2}$
$3NO_2 + BaO \cdot bulk \rightarrow Ba(NO_3)_2 \cdot bulk + NO$	$R_{29}^{NSRC} = k_{29}^{NSRC}\, \Psi_{NO_{xb}}^{cap}\, y_{NO_2}\, (\psi_{NO_{xb}}^{eq} - \psi_{NO_{xb}})^2$ [a]
$Ba(NO_3)_2 \cdot bulk \rightarrow Ba(NO_3)_2$	$R_{30}^{NSRC} = k_{30}^{NSRC}\, \Psi_{NO_{xb}}^{cap}\, (\psi_{NO_{xb}} - \psi_{NO_x})$

$G_1 = (1 + K_{inh,1}\, y_{CO} + K_{inh,2}\, y_{C_2H_6})^2 \cdot (1 + K_{inh,3}\, y_{CO}^2\, y_{C_2H_6}^2) \cdot (1 + K_{inh,4}\, y_{NO_x}^{0.7})\, T^s$, $G_2 = 1 + K_{inh,5}\, y_{CO_2}$, $G_3 = 1 + K_{inh,6}\, y_{CO_2}$,
$G_4 = (1 + 0.1\, K_{inh,6}\, y_{CO_2})\, (1 + K_{inh,7}\, y_{NO_x})$, $G_5 = 1 + K_{inh,8}\, y_{CO}$, $G_6 = (1 + K_{inh,9} y_{CO})\, (1 + K_{inh,10} y_{C_2H_6})$.

[a] The reaction rates R_{16}^{NSRC}, R_{17}^{NSRC}, and R_{29}^{NSRC} are multiplied by $[sgn(\psi_{NO_x}^{eq} - \psi_{NO_x})]$, i.e., by −1 or +1 to obtain correct sign of the reaction rate in the case $(\psi_{NO_x} > \psi_{NO_x}^{eq})$.

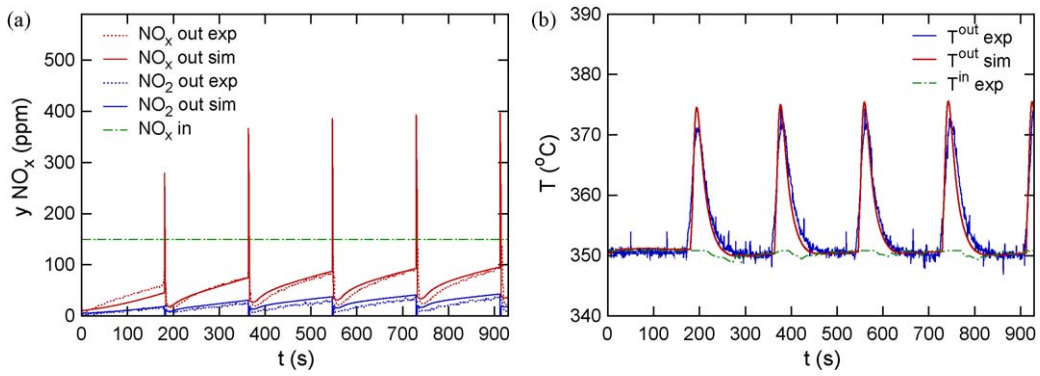

Fig. 3. Typical evolution of outlet NO_x concentrations (a) and temperatures (b) during periodic lean/rich NSRC operation. Quasi-adiabatic lab reactor (cf. Table 1), $\tau_{lean} = 180$ s, $\tau_{rich} = 3$ s, $SV = 60\,000\ h^{-1}$, $T^{in} = 350\,^{\circ}C$. Lean inlet gas: 9.5% O_2, 150 ppm NO. Rich inlet gas: 1.9% O_2, 3.3% CO, 1.1% H_2, 3000 ppm C_3H_6, 150 ppm NO. Always 7.0% H_2O, 7.0% CO_2, balance N_2.

NO_2 by CO and/or HC back to NO (observed at low temperatures below the light-off of the CO+O_2 and HC+O_2 reactions) has been newly included in this work to predict correctly the NO_2 concentrations during cold start periods (cf. R_{10}^{NSRC} and R_{11}^{NSRC}). Transient oxygen storage and reduction effects are included in the form of reactions R_{12}^{NSRC}–R_{15}^{NSRC}. The oxygen storage affects the balance of the reducing agents during the NSRC regeneration [28].

Both NO_2 and NO adsorption pathways are considered on the NO_x storage sites close to dispersed noble metals, where oxidation of the adsorbed NO_x to surface nitrates can proceed with oxygen (the summary reactions R_{14}^{NSRC} and R_{15}^{NSRC}, respectively). Additional NO_x storage is considered on the bulk sites that are not in contact with noble metals (reaction R_{29}^{NSRC}). Here gaseous NO_2 is required for oxidation of the adsorbed NO_x to nitrates, resulting in the NO_2 disproportion stoichiometry (two molecules NO_2 stored, one reduced back to NO).

During the regeneration the following primary processes are considered: "direct" reduction of the stored NO_x enabled by spill-over to the noble metal sites (reactions R_{18}^{NSRC}–R_{21}^{NSRC}), and desorption of the stored NO_x in the form of NO (reactions R_{22}^{NSRC}–R_{24}^{NSRC}). The desorbed NO can be then reduced over noble metal sites (reactions R_{6}^{NSRC}–R_{8}^{NSRC}). The reduction of the stored NO_x is considered to give NH_3 in reaction with hydrogen (R_{20}^{NSRC}), while N_2 is formed in reaction with C_3H_6 (R_{21}^{NSRC}). In the case of CO, formation of both NH_3 (in presence of water) and N_2 is possible (reactions R_{18}^{NSRC}–R_{19}^{NSRC}), cf. [18]. The formed ammonia can be consequently oxidised to nitrogen by the reactions with NO_x or oxygen accumulated on the catalyst surface or coming from the inlet gas (reactions R_{25}^{NSRC}–R_{28}^{NSRC}). Reduction of the NO_x from the bulk storage sites is treated via formal spill-over to standard NO_x storage sites (reaction R_{30}^{NSRC}). Here eventual additional resistance of the bulk NO_x storage sites to regeneration is described by a single parameter (k_{30}^{NSRC}) to avoid a further increase of model reactions and parameters that would be necessary in the case of a strictly separated regeneration of each NO_x storage site type. It needs to be mentioned here that the NH_3 formation dynamics in our model are not primarily a consequence of "slow" NO_x storage sites, but it is a result of the interplay between the NH_3 formation and consumption in the spatially distributed system, as it was demonstrated in the simulations with the NO_x storage sites of a single type [28].

In our prior work [18], the NSRC model parameters were evaluated with a de-greened commercial catalyst of the type PtRh/Ba/Ce/γ-Al_2O_3 and the model was validated by driving cycle data. In this paper we will demonstrate the use of the model with an extensively aged NSRC monolith of similar type. The catalyst was aged during real driving conditions (160 000 km, including 120 desulfation runs and 200 DPF regenerations, as the catalyst was part of a combined aftertreatment system). Based on our experience we can conclude that the studied NSRC catalyst possessed roughly (1/2) of the effective NO_x storage capacity usual for de-greened NSRC catalysts. The kinetic parameters of the aged catalyst were adjusted according to lab experiments with mixtures of synthetic gases (CO, H_2, C_3H_6, O_2, NO, NO_2, CO_2, H_2O, and N_2). Values from the previous NSRC calibration were used as initial estimates.

The parameters were evaluated separately in several subsets as described in [37,38,18]. The effects of individual reducing agents (CO, H_2, HC) were not studied separately again as it was done in prior work [18]. Instead, the ratio of their activity determined with the fresh catalyst was kept constant when evaluating the kinetic parameters with the complete reducing mixture.

The experiments were done in a quasi-adiabatic lab reactor, still commonly used in the automotive industry. This configuration is obviously much less suitable for the evaluation of kinetic parameters than a nearly isothermal monolith slice [18] or powder microreactor [39]. Geometry of the studied NSRC monolith sample is given in Table 1. The used diameter of the monolith section (25 mm) resulted in quasi-adiabatic conditions with non-negligible heat losses. To approximate actual evolution of temperatures in the lab reactor, an effective heat loss coefficient Ω was implemented into the enthalpy balance of the solid phase, cf. Eq. (5). During the lab experiments, the NSRC sample was placed in an oven where the surrounding temperature T^e was equal to the inlet gas temperature T^{in}. However, during the operation of full-size monoliths the heat losses are negligible and $\Omega = 0$ is used.

Typical evolution of the NSRC outlet concentrations and temperatures during periodic lean/rich experiment is given in Fig. 3. The NSRC was regenerated at 400 °C before the experiment. Gradual stabilisation of the outlet NO_x concentrations during the periodic operation can be seen in Fig. 3a — the NO_x reduction within the short rich phase is not complete and the residual NO_x coverage decreases the efficiency of the NO_x adsorption in the next lean phase. High CO, H_2 and HC concentrations are present in the system during the rich phase, together with a lower, but still substantial level of oxygen. This results in an extensive heat evolution that is reflected by the outlet temperature peaks in Fig. 3b (with certain delay caused by heat accumulation and conduction). The temperature increase further accelerates reaction rates and helps to regenerate the NO_x storage catalyst.

Examples of the measured and simulated NO_x and NH_3 concentrations at the NSRC outlet during stabilised lean/rich cycles are shown in Fig. 4. Almost no delay of the outlet NH_3 peak in the rich phase is observed until 350 °C (cf. Fig. 4a). This is a significant difference in comparison with the just de-greened NSRC studied in [18] where an increasing delay of the NH_3 peak was

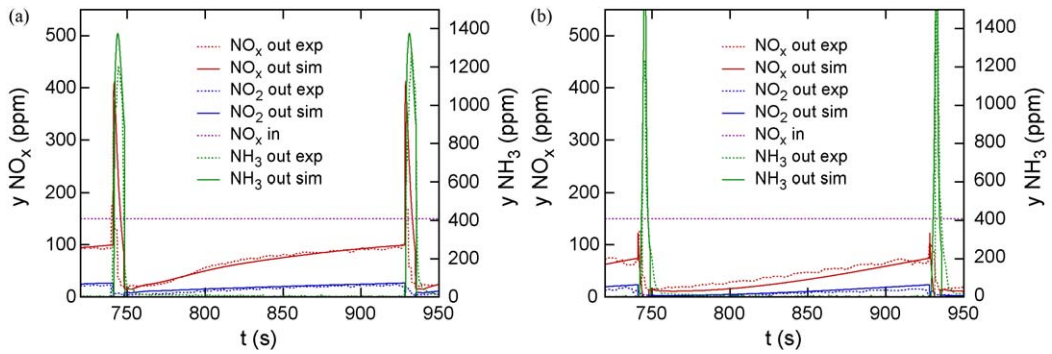

Fig. 4. Experimentally observed and simulated evolution of the outlet NO_x and NH_3 concentrations during periodic lean (180 s)/rich (7 s) operation with the aged NSRC. (a) $T^{in} = 300\,^{\circ}C$, (b) $T^{in} = 450\,^{\circ}C$. Quasi-adiabatic lab reactor (cf. Table 1), $SV = 60\,000\,h^{-1}$. Lean inlet gas: 9.5% O_2, 150 ppm NO. Rich inlet gas: 1.9% O_2, 3.3% CO, 1.1% H_2, 3000 ppm C_3H_6, 150 ppm NO. Always 7.0% H_2O, 7.0% CO_2, balance N_2.

observed already above 200 °C. Based on the simulation analysis we assume that two effects play roles here: (i) lower NO_x and oxygen storage capacity of the aged NSRC, and (ii) lower activity of noble metals in the aged NSRC. The lower noble metal and oxygen storage activities correspond to the shifted light-off of the ammonia oxidation reactions (that are the main reason for the ammonia peak delay) to higher temperatures – a typically delayed and narrowed NH_3 peak can be observed only at $T > 400\,^{\circ}C$ (cf. Fig. 4b).

When comparing the simulated regeneration of the fresh and aged NSRC at the same temperature, the reactions are generally slower with the aged NSRC so that the resulting spatial concentration gradients inside the reactor are milder, and the moving boundary region between the reduced and oxidised part of the monolith is more widely distributed along the reactor, which again supports the faster NH_3 breakthrough. A typical reduction front with steep concentration gradients (cf. [28,18]) is established in the aged NSRC only at higher temperatures.

All these effects contribute to the higher NH_3 yields in the aged NSRC, furthermore observed in a wider range of temperatures (cf. Fig. 5). With the just de-greened NSRC studied in [18], the maximum NH_3 yield was observed already at 200 °C while in Fig. 5 we can find it around 350 °C.

The lower noble metals activity and possibly a worse contact with the NO_x storage material in the aged NSRC hinder the reduction of the stored NO_x at lower temperatures. It results in a relatively slow increase of the integral NO_x conversion with temperature (cf. Fig. 5). Generally, the maximum NO_x conversion

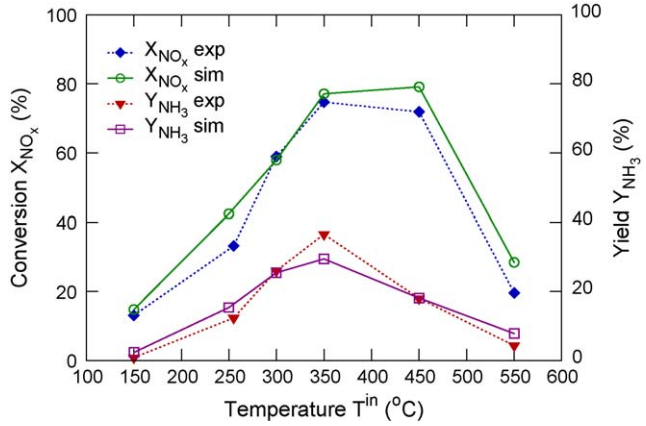

Fig. 5. Integral NO_x conversions X_{NOx} and NH_3 yields Y_{NH_3} during periodic lean (180 s)/rich (7 s) operation of the aged NSRC, in dependence on the inlet gas temperature T^{in} (quasi-adiabatic lab reactor, cf. Table 1). Lean inlet gas: 9.5% O_2, 150 ppm NO. Rich inlet gas: 1.9% O_2, 3.3% CO, 1.1% H_2, 3000 ppm C_3H_6, 150 ppm NO. Always 7.0% H_2O, 7.0% CO_2, balance N_2, $SV = 60,000\,h^{-1}$.

in the aged NSRC is shifted to higher temperatures with the aged NSRC, as well as the maximum NH_3 yield. However, the high temperature limit of the NSRC operation remains the same, determined by a decrease of the NO_x storage capacity due to thermal instability of the adsorbed NO_x [10]. Thus, the optimum temperature window of the aged NSRC is narrower.

After the discussed adjustment of reaction rate coefficients and effective oxygen and NO_x storage capacities, the presented NSRC model was able to describe and predict the dynamic behaviour of both de-greened and aged NSRC in wide range of operating conditions. For the NSRC + SCR simulations presented in this paper the aged NSRC was considered.

4. Selective catalytic reduction (SCR) of NO_x by NH_3

In recent years the automotive application of NH_3-SCR systems motivated fundamental investigations of both the standard and fast SCR reaction mechanisms [40–42,22,43]. With respect to reaction mechanisms and modeling of their kinetics, it seems that a similar approach can be used for the global modeling of the catalytic processes on the most commonly used SCR materials like $V_2O_3-WO_3/TiO_2$, Fe-ZSM5 and Cu-ZSM5 [20,44,45]. The global SCR reaction kinetics presented in Table 3 are based on an extensive study of the reaction mechanisms on SCR catalysts of the types $V_2O_3-WO_3/TiO_2$ [21,46] and Fe-ZSM5 [22].

The first step in the SCR reaction is the adsorption and storage of NH_3 onto the catalyst (R_1^{SCR} and R_2^{SCR}). For the reaction rates a non-activated NH_3 adsorption process and a Temkin-type NH_3 desorption is assumed [47]. By means of simple Arrhenius expression (R_3^{SCR}) the NH_3 oxidation is accounted for. Also a small activity regarding NO oxidation to NO_2 can usually be found on automotive SCR catalysts, which is modeled by the rate expression R_4^{SCR} taking into account the NO/NO_2 thermodynamic equilibrium [20].

The rate law for the so-called "standard" SCR reaction (R_5^{SCR}) is based on a dual-site modified redox (MR) rate law [21]. The main assumption is that two different types of sites are present on the catalyst surface: acidic non-reducible sites for NH_3 adsorption (denoted by *, with NH_3^* coverage θ_{NH_3}, and the sites concentration $\Psi_{NH_3}^{cap}$), and redox sites for NO + NH_3^* activation/reaction (denoted by x, with NH_3^x coverage σ_{NH_3}, and the sites concentration Ψ_x^{cap}). It is further assumed that NH_3 can block the active redox sites (x), leading to NH_3 inhibition of the "standard" SCR reaction.

An equilibrium state of the NH_3 spill-over from the acidic sites (*) sites to the redox (x) sites can be assumed for many SCR technologies. However, it has been revealed that this assumption is not valid for the Fe-ZSM5 SCR technology used within this study. Therefore a finite $NH_3^* \rightleftharpoons NH_3^x$ spill-over rate (R_{10}^{SCR}) needs to be introduced [21]. Based on dynamic experiments with NH_3 dosing

Table 3
Reactions on Fe-ZSM catalyst for selective NO_x reduction by NH_3 (SCR) – derived from [19–22]. Local molar concentrations c^s in washcoat pores are considered in all reactions – the superscript "s" was omitted below for the sake of brevity.

Reaction step	Reaction rate
$NH_3 + * \rightarrow NH_3^*$	$R_1^{SCR} = k_1^{SCR}\,\Psi_{NH_3}^{cap}\,c_{NH_3}(1-\theta_{NH_3})$
$NH_3^* \rightarrow NH_3 + *$	$R_2^{SCR} = k_{0,2}^{SCR}\,\Psi_{NH_3}^{cap}\exp[-E_{a,2}^{SCR}(1-\gamma\,\theta_{NH_3})/(R^g\,T^s)]\,\theta_{NH_3}$
$4NH_3^* + 3O_2 \rightarrow 2N_2 + 6H_2O$	$R_3^{SCR} = k_3^{SCR}\,\Psi_{NH_3}^{cap}\,\theta_{NH_3}\,[y_{O_2}^{\beta_3}]$
$NO + (1/2)O_2 \rightleftharpoons NO_2$	$R_4^{SCR} = k_4^{SCR}\,(c_{NO}\,c_{CO_2}^{0.5} - c_{NO_2}/K_4^{eq})\,[y_{H_2O}^{\beta_4}]$
$4NH_3^* + 4NO + O_2 \rightarrow 4N_2 + 6H_2O$	$R_5^{SCR} = k_5^{SCR}\Psi_{NH_3}^{cap}\,\Psi_x^{cap}\,c_{NO}\,y_{O_2}^{\beta_5}\theta_{NH_3}(1-\sigma_{NH_3})$
$4NH_3^* + 2NO + 2NO_2 \rightarrow 4N_2 + 6H_2O$	$R_6^{SCR} = k_6^{SCR}\,\Psi_{NH_3}^{cap}\,c_{NO}\,c_{NO_2}\,\theta_{NH_3}\,[y_{H_2O}^{\beta_6}]$
$2NH_3^* + 2NO_2 \rightarrow NH_4NO_3\uparrow + N_2 + H_2O$	$R_7^{SCR} = k_7^{SCR}\,\Psi_{NH_3}^{cap}\,c_{NO_2}^2\,\theta_{NH_3}$
$2NH_3^* + 2NO_2 \rightarrow N_2O + N_2 + 3H_2O$	$R_8^{SCR} = k_8^{SCR}\,\Psi_{NH_3}^{cap}\,c_{NO_2}\,\theta_{NH_3}$
$2NH_3^* + (3/2)NO_2 \rightarrow (7/4)N_2 + 3H_2O$	$R_9^{SCR} = k_9^{SCR}\,\Psi_{NH_3}^{cap}\,c_{NO_2}\,\theta_{NH_3}$
$NH_3^* + x \rightleftharpoons NH_3^x + *$	$R_{10}^{SCR} = k_{10}^{SCR}\,\Psi_{NH_3}^{cap}\,\Psi_x^{cap}\,[\theta_{NH_3}(1-\sigma_{NH_3}) - \sigma_{NH_3}(1-\theta_{NH_3})/K_{LH}]$

The factors $[y_{O_2}^{\beta_3}]$, $[y_{H_2O}^{\beta_4}]$ and $[y_{H_2O}^{\beta_6}]$ were used only for scaling the reaction rates from the lab experiments with lower O_2 and H_2O concentrations (2% and 3%, respectively) to the high O_2 and H_2O concentrations observed in Diesel exhaust gas ($\approx$10%). At the high O_2 and H_2O concentrations a saturation level is achieved so that zero reaction orders β_3, β_4 and β_6 are used.

(discussed in more detail below), the mutual concentration ratio of the two surface sites in the studied Fe-ZSM5 catalyst was estimated to be 450:1 ($\Psi_{NH_3}^{cap} : \Psi_x^{cap}$). This is consistent with the fact that in the zeolite structure there are much more NH_3-adsorptions sites than the reactive sites (that are here correlated with Fe).

The partial conversion of NO to NO_2 in the upstream NSRC leads to a higher NO_x conversion rate in the SCR. This is due to the so-called "fast" SCR reaction (R_6^{SCR}). However, high NO_2/NO_x ratios can result in the formation of NH_4NO_3 and N_2O which is accounted for by R_7^{SCR} and R_8^{SCR}, respectively. In the presented model it is assumed that NH_4NO_3 goes directly into the gas phase, which is true only for temperatures higher than 200 °C. A more detailed approach to NH_4NO_3 formation with high NO_2 concentrations was discussed in [48]. It should be noted that NH_4NO_3 is not solely a by-product, because recent findings have pointed out that nitrates and nitrites on the surface play an important role in the overall SCR mechanism [41,46,22,49,50]. Finally, NO_2 can react directly with NH_3 (R_9^{SCR}) — this reaction is significant only at higher temperatures.

Transient response measurements (TRM) were conducted to obtain calibration data. In order to avoid any transport effects, a powder microreactor, using a crushed commercial Fe-ZSM5 catalyst (cf. Table 1) was used for the kinetic experiments. A hydro-thermal (HT) conditioning was applied for 5 h at 600 °C prior the measurements to de-green the catalyst. A typical example of a TRM experiment is depicted in Fig. 6 where the NH_3 adsorption/desorption dynamics is studied. More details about the experimental and calibration procedure can be found in [1,20].

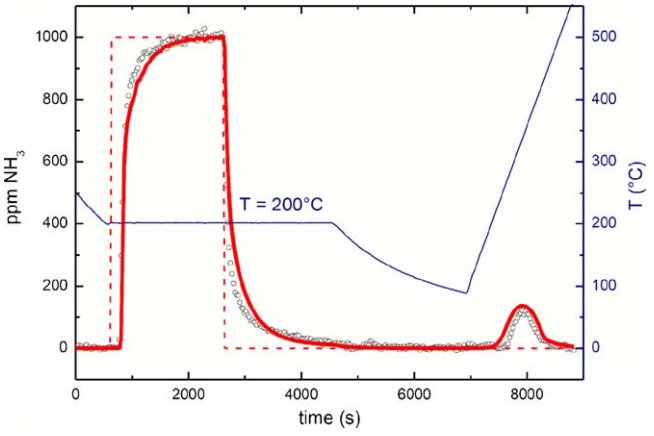

Fig. 6. NH_3 adsorption/desorption experiment at 200 °C with the crushed SCR monolith powder. Dashed line: NH_3 inlet concentration, open circles: measured NH_3 outlet concentration, solid line: simulated NH_3 outlet concentration. Inlet gas composition: 0/1000 ppm NH_3, 2% O_2, 3% H_2O, balance He.

After the calibration the model is able to predict the NO_x conversion and selectivity in a wide range of operation conditions. Fig. 7a–d depicts comparisons between measured and simulated powder microreactor outlet concentrations for various NO_2/NO_x inlet feed ratios in the temperature range from 180 °C to 550 °C. Some deviations can be noted for high NO_2/NO_x ratios and temperatures below 200 °C. Under those conditions formation and storage of NH_4NO_3 plays an important role [22,48] which is not treated in detail in the model used for the present study (Table 3).

The Fe-ZSM5 catalyst studied in this work possesses a significant NH_3 inhibition effect. As an example, Fig. 8 depicts the dynamic response of the microreactor outlet by applying 300 s NH_3 pulses. The start of NH_3 dosing is indicated by the decrease of the NO_x concentration at the reactor outlet. The decrease of the NH_3 concentration at the reactor outlet indicates the NH_3 shut off. It can be noted that the steady state NO_x conversion is lower compared to the levels during the NH_3 shut off/on phases. This can be explained by the fact that the build-up of the stored NH_3 led to an increasing inhibition of the SCR reaction. After removing NH_3 from the feed, the stored NH_3 is consumed by the SCR reaction, which reduces the inhibition effect and leads to an increased reaction rate until the stored NH_3 is completely consumed.

The comparison between simulations and experiments for a full-scale SCR monolith is shown in Fig. 9a. During these engine test bench measurements, the engine was running at constant speed and load. Around the time 750 s, ammonia was injected in excess into the exhaust line. As a result, the NO_x concentration at the SCR outlet decreased. However, after a certain time the NO_x outlet concentration increased partly. Thus, similar dynamic features like in the laboratory experiment (Fig. 8) are observed, which confirms the practical relevance of the NH_3 inhibition effect.

The comparison of Fig. 9a and b underlines the influence of the NH_3 spill-over reaction (R_{10}^{SCR}). The simulation data in Fig. 9a are calculated using the reaction kinetics listed in Table 3. However, Fig. 9b depicts the situation when equilibrium with respect to the $NH_3^* \rightleftharpoons NH_3^x$ spill-over is assumed in the SCR model. Under this assumption all the rate laws used for the simulations remain

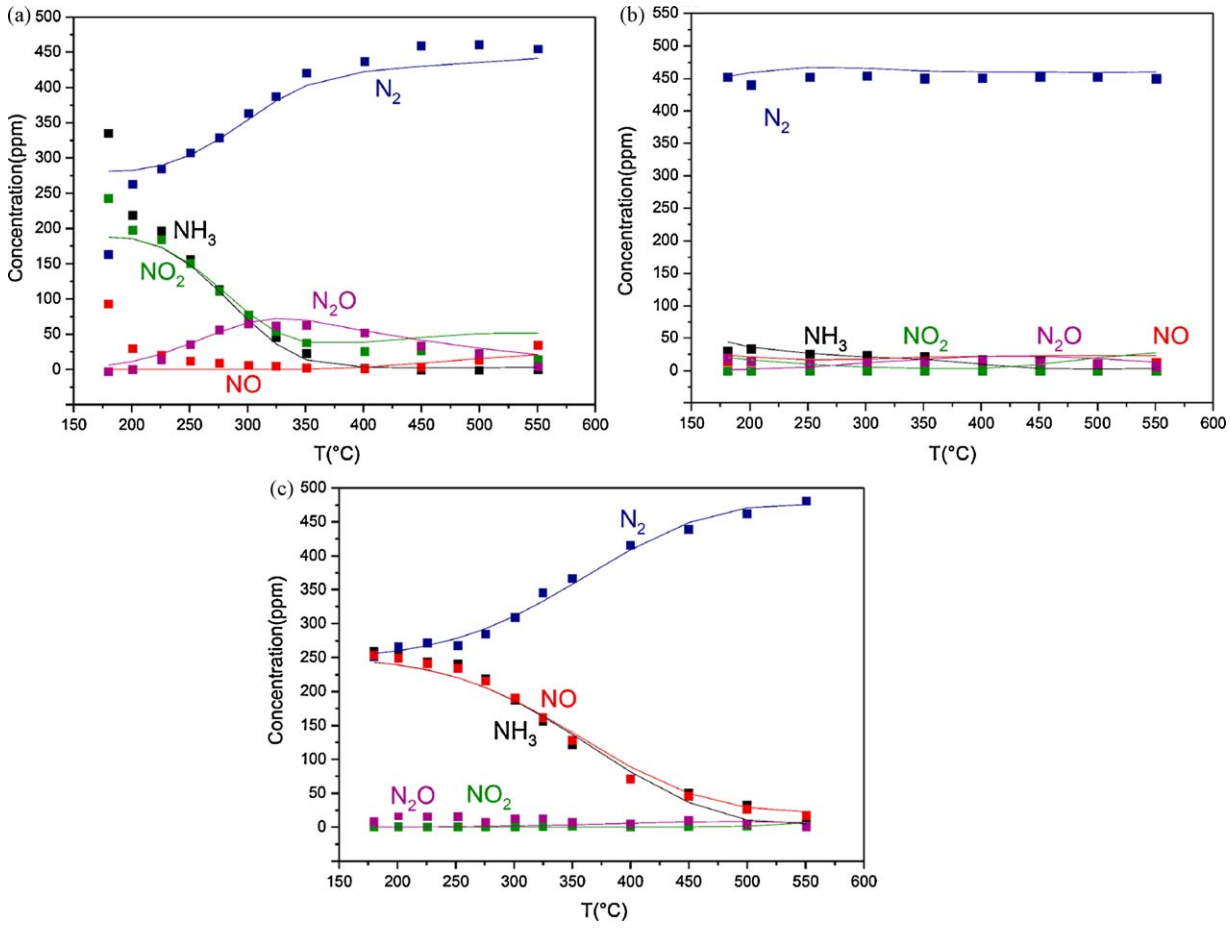

Fig. 7. Steady state outlet concentrations in a microreactor with the crushed SCR monolith for varying NO_2/NO_x inlet concentration ratios. Symbols: experimental data, lines: simulations. Inlet gas composition: 500 ppm NO_x, 500 ppm NH_3, 3% H_2O, 2% O_2, balance He. The $y^{in}_{NO_2}/y^{in}_{NO_x}$ ratios: (a) 0.75, (b) 0.50, (c) 0.25.

identical to Table 3, but the R^{SCR}_{10} is omitted and the "standard" SCR reaction rate R^{SCR}_{5} becomes [20,21]:

$$R^{SCR}_{5,eq.spill} = \frac{k^{SCR}_5 c_{NO} y^{\beta_5}_{O_2} \theta_{NH_3}}{[1 + K_{LH}\theta_{NH_3}/(1-\theta_{NH_3})]} \quad (13)$$

The simulation results indicate clearly that only the assumption of a finite spill-over reaction rate is able to reproduce the transient NH_3 inhibition effects with the Fe-ZSM5 catalysts. However, based on our experience, for many other SCR technologies the assumption of an equilibrium state regarding the $NH_3^* \rightleftharpoons NH_3^x$ spill-over

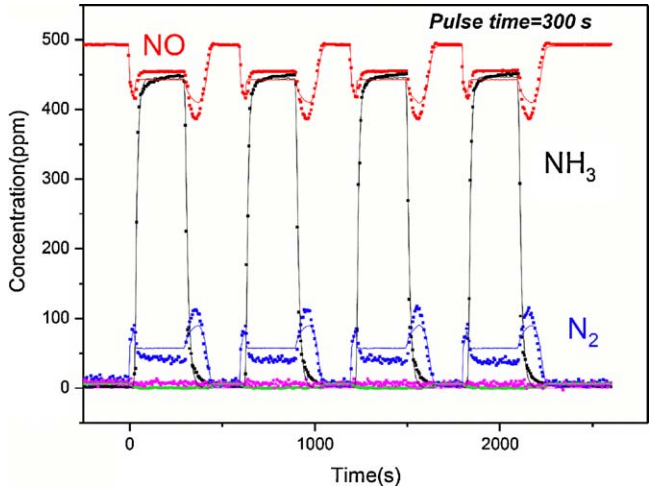

Fig. 8. Outlet concentrations during a dynamic NH_3 dosing experiment in a microreactor with the crushed SCR monolith. Symbols: measurement, lines: simulation (including the NH_3 spill-over reaction at finite rate). $T = 250\,^{\circ}C$, inlet gas concentrations: 500 ppm NO, 0/500 ppm NH_3 (periodic alternation each 300 s), 2% O_2, 3% H_2O, balance He.

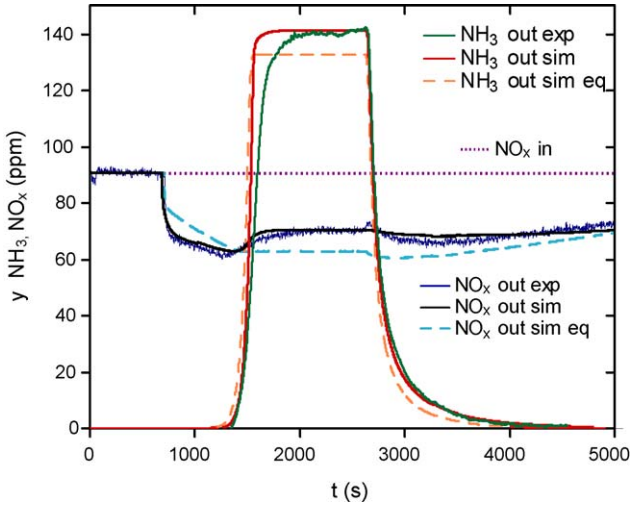

Fig. 9. Outlet concentrations during an engine test bench experiment with a full-size Fe-ZSM5 SCR monolith (400 cpsi, 7 mil, pre-conditioned hydro-thermally 5 h at 600 °C). $T^{in} = 200\,^{\circ}C$, $SV = 20\,000\,h^{-1}$, $y^{in}_{NO_2}/y^{in}_{NO_x} = 0.055$, $y^{in}_{NH_3}/y^{in}_{NO_x} = 1.77$. The ammonia is added into the inlet stream in the period $t = 700$–2600 s. Label "sim" denotes simulation with the NH_3 spill-over reaction at a finite rate. Label "sim eq" denotes simulation with the NH_3 spill-over equilibrium.

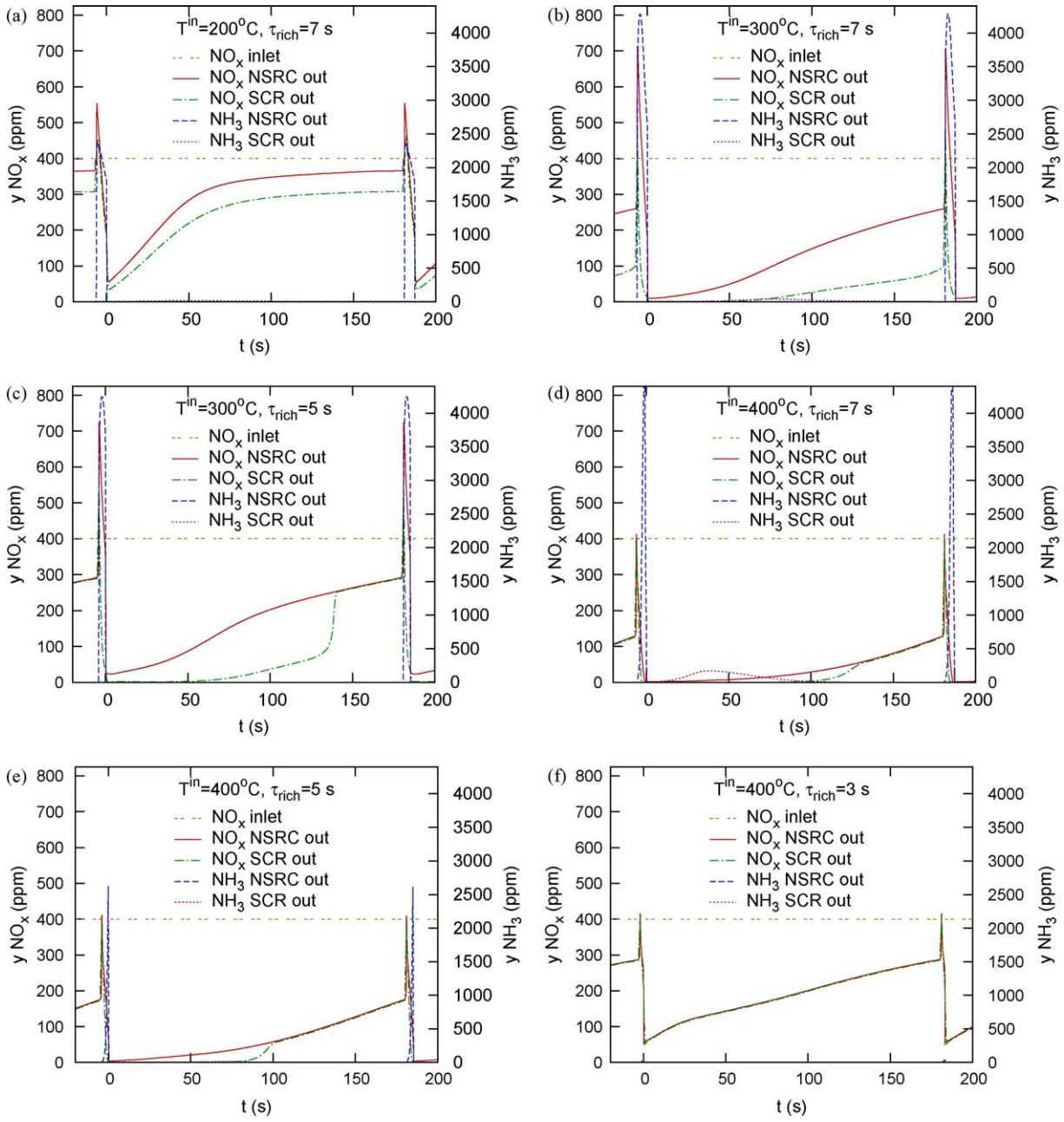

Fig. 10. Evolution of NO_x and NH_3 concentrations in the NSRC + SCR system during stabilised lean/rich cycling with $\tau_{lean} = 180$ s at several different inlet temperatures T^{in} and rich phase lengths τ_{rich}. Lean inlet gas: 12% O_2, 400 ppm CO, 0 ppm H_2, 60 ppm C_3H_6, 400 ppm NO_x (300 ppm NO + 100 ppm NO_2). Rich inlet gas: 0.7% O_2, 2.5% CO, 1.5% H_2, 3000 ppm C_3H_6, 400 ppm NO_x (400 ppm NO + 0 ppmNO_2). Always 10.0% H_2O, 7.0% CO_2, balance N_2, $SV = 35\,000\,h^{-1}$.

reaction is acceptable. Furthermore, with the CU-ZSM5 catalyst the NH_3 inhibition is generally less pronounced [45] and that leads to very low or zero K_{LH} in Eq. (13). In the simulations of the combined NSRC + SCR system presented in the following section, we consider the Fe-ZSM5 SCR catalyst so that the complete reaction rates listed in Table 3 have been used.

5. Combined NSRC + SCR system

A simulation study of the combined NSRC + SCR system was performed for two adiabatic full-size monoliths (cf. Table 1; the aged NSRC was considered). If not stated otherwise, the monoliths were located closely one after another. Performance of the system was evaluated first in defined periodic lean/rich operation for selected temperatures and rich phase lengths, and then in European test driving cycles EUDC [2].

Examples of the simulation results for defined periodic lean/rich operation can be seen in Fig. 10. The NSRC + SCR system was tested with a relatively high inlet NO_x level (400 ppm) to investigate critically the trends in the NO_x conversion – higher conversions would be achieved in a wider range of operating conditions with a lower NO_x feed. At low operating temperatures ($T^{in} = 200\,°C$, Fig. 10a) the reduction of the stored NO_x in the aged NSRC is quite slow and inefficient even with relatively long regeneration (7 s). The incomplete NSRC regeneration results in quite high NO_x breakthrough during the lean phase. A certain amount of ammonia is formed in the NSRC already at this lower temperature. The adsorption of the generated NH_3 in the SCR is complete, and the adsorbed ammonia is utilised in additional NO_x reduction in the SCR during the lean phase, improving the overall NO_x conversion.

At intermediate operating temperatures ($T^{in} = 300\,°C$) with the same regeneration (7 s), the NO_x reduction in the NSRC is much

more effective, which is reflected in lower NO_x breakthrough during the lean phase (Fig. 10b). The higher NO_x reduction rate together with still relatively low rate of the NH_3 oxidation in the aged NSRC lead to a large NH_3 peak (the operating conditions are close to those with maximum NH_3 yield shown in Fig. 5). However, the downstream SCR is still able to adsorb the ammonia almost completely (only few ppm of desorbed NH_3 can be seen in the consequent lean phase). The NH_3-SCR reduces here the NO_x emissions to a large extent. With a shorter rich phase at the same temperature (5 s, Fig. 10c) the NO_x conversions in the NSRC are slightly lower and less NH_3 is produced. This leads to depletion of the NH_3 stored in the SCR catalyst already approximately 50 s before the end of the lean phase, and from this point the SCR gives no additional NO_x conversion (Fig. 10c).

At high operating temperatures ($T^{in} = 400\,^{\circ}C$, Fig. 10d), a facile NO_x reduction during the rich phase is achieved even with the extensively aged NSRC catalyst, and the effect of the SCR monolith on the NO_x conversion is rather small. It can be seen in Fig. 10d that in contrast to the lower temperatures, the NH_3 peak at the NSRC outlet is significantly narrower and delayed, so that the NH_3 yield is lower. This indicates the regeneration regime with developed steep internal concentration gradients and fast NH_3 re-oxidation inside the NSRC [28,18]. The NH_3 peak emitted from the NSRC is still temporarily adsorbed in the SCR, however, we can observe a partial NH_3 desorption later in the lean phase. This is caused by two effects: (i) the effective NH_3 adsorption capacity of the SCR catalyst decreases with temperature, (ii) the NO_x levels leaving NSRC during the first part of the lean phase are very low, i.e., the adsorbed ammonia is in local excess. The temperature wave originating from the NSRC regeneration (similar to that shown in Fig. 3) needs to be also taken into account with respect to NH_3 desorption from the SCR monolith. In the complete DOC+NSRC+DPF+SCR system (Fig. 2), the SCR is not located closely to the NSRC but in the underfloor position so that the temperature peaks from the NSRC regenerations are quite well dissipated before reaching the SCR. In this situation the separated NSRC and SCR converters are more advantageous than an integrated NSRC/SCR catalyst.

The situation for the shorter 5 and 3 s rich phases at the high temperature is depicted in Fig. 10e and f, respectively. It can be seen that at the given conditions the 5 s rich phase (Fig. 10e) is more favourable than the 7 s one (Fig. 10d) – the NO_x conversions are similar and less NH_3 is emitted. The shorter rich phase means also a lower fuel consumption penalty corresponding to the enrichment, as well as a lower CO and HC breakthrough. With the

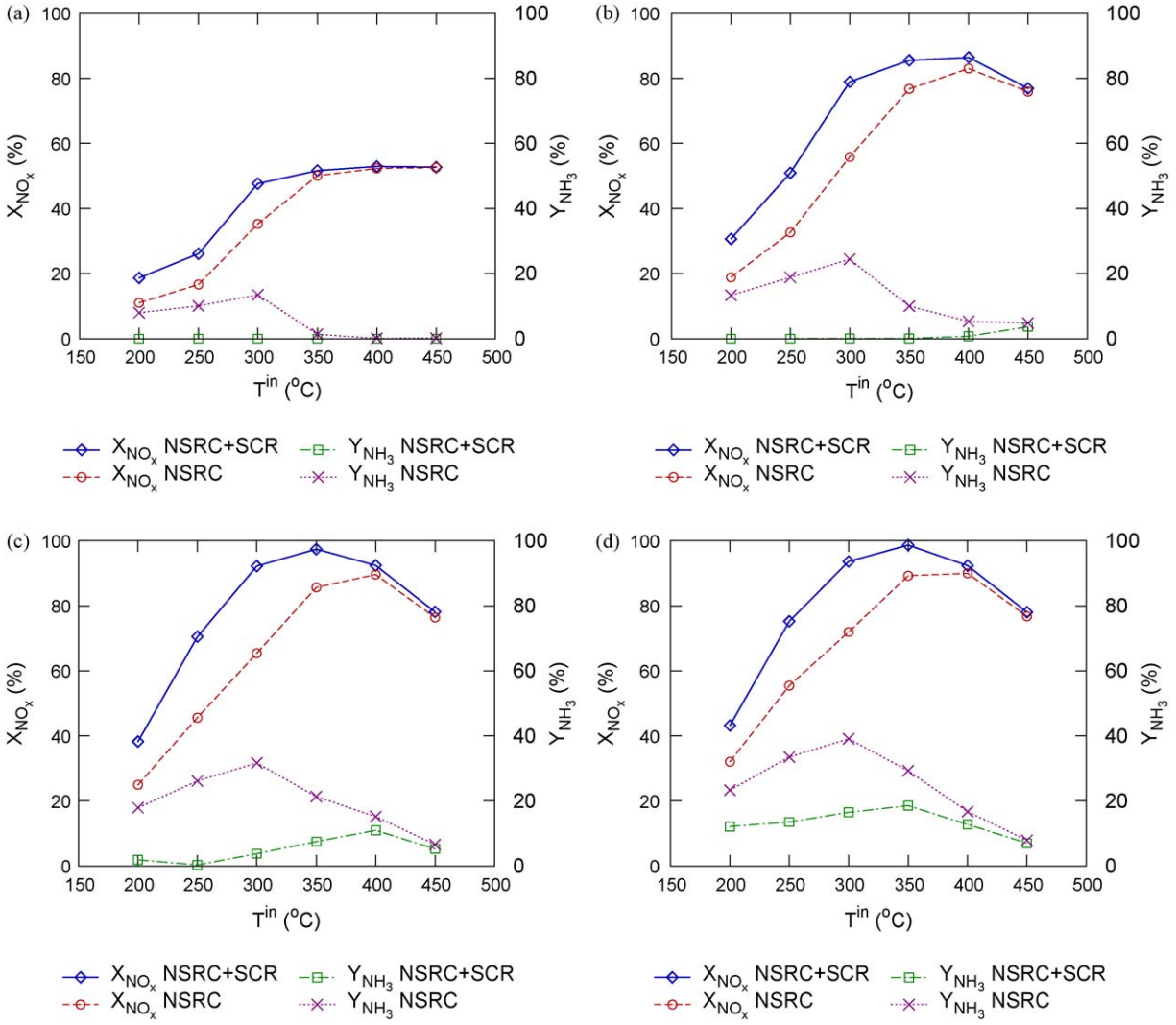

Fig. 11. Integral NO_x conversions and NH_3 yields in the NSRC + SCR system during stabilised lean/rich cycling with $\tau_{lean} = 180$ s, dependence on inlet temperature T^{in}. Adiabatic full-size NSRC and full-size SCR in series (cf. Table 1). (a) $\tau_{rich} = 3$ s, (b) $\tau_{rich} = 5$ s, (c) $\tau_{rich} = 7$ s, (d) $\tau_{rich} = 10$ s. Lean inlet gas: 12% O_2, 400 ppm CO, 0 ppm H_2, 60 ppm C_3H_6, 400 ppm NO_x (300 ppmNO + 100 ppmNO_2). Rich inlet gas: 0.7% O_2, 2.5% CO, 1.5% H_2, 3000 ppm C_3H_6, 400 ppm NO_x (400 ppmNO + 0 ppmNO_2). Always 10.0% H_2O, 7.0% CO_2, balance N_2, $SV = 35\,000\ h^{-1}$.

developed regeneration front inside the monolith, the CO and HC breakthrough peaks appear at the NSRC outlet approximately at the same time as the ammonia [18,28].

With the shortest 3 s rich phase (Fig. 10f), we can observe no NH_3 peak at the NSRC outlet, indicating that in this case the regeneration was stopped before the reduction front passed along the entire NSRC monolith. This incomplete regeneration though results in a higher NO_x breakthrough during the lean phase.

Calculated dependences of integral NO_x conversions and NH_3 yields on the inlet gas temperature are given in Fig. 11. With the shortest regeneration phase (Fig. 11a) the NO_x conversion in the NSRC is low and NH_3 is generated only below 350 °C. All the ammonia is then utilised in the SCR, leading to improvement of the NO_x conversions at lower temperatures.

With the intermediate rich phase length (Fig. 11b), the NO_x conversion in the NSRC improves, and generally more NH_3 is generated, certain amounts even above 350 °C. The formed NH_3 is again utilised in the SCR for additional NO_x conversion, so that a good overall deNO_x efficiency is achieved in the temperature range 300–450 °C. Only at the highest temperature a minor ammonia slip is predicted. At the temperatures above 500 °C, the NSRC operation becomes limited by the loss of NO_x storage capacity, so that the NO_x conversion decreases, and also the selectivity towards ammonia is low.

When a longer rich phase is applied (Fig. 11c), the NO_x conversions increase further (maximum more than 95%), however, a noticeable NH_3 breakthrough can be observed above 300 °C. Around 350 °C it is caused by a local excess of the NH_3 over the NO_x in the SCR – the NO_x reduction in the NSRC alone is so effective that only small NO_x amounts are passed to the SCR, and therefore a part of the formed NH_3 remains unused.

It can be seen that with the longest regenerations (Fig. 11d), the NO_x conversions improve further only in a minimum extent because almost complete NSRC regeneration was achieved already within a shorter rich phase. Furthermore, too much NH_3 is generated that cannot be utilised in the SCR.

The shown trends of the overall NO_x conversions in the combined NSRC + SCR aftertreatment system are in a good agreement with the results obtained experimentally by other researchers [17,51]. In reference [51], the positive effect of the SCR was limited to lower temperatures, which is consistent with the fact that a fresh/de-greened NSRC catalyst was used and the NSRC was regenerated by hydrogen – such a system exhibits maximum NH_3 yield at much lower temperatures than the aged NSRC regenerated by a mixture of CO, H_2 and HC.

Evolution of temperatures together with the NO_x and NH_3 concentrations in the combined NSRC + SCR system during the five times repeated EUDC (5×400 s) cycle is given in Fig. 12. The EUDC test driving cycle is the standard European cycle for extra-urban driving (i.e., higher speeds), cf. e.g. [2]. Two exhaust gas enrichments were applied in each EUDC cycle. Each regeneration lasted 3 s, but at approximately two times higher SV than in Figs. 10 and 11. The enrichments lead to the NSRC regeneration accompanied by the NH_3 formation.

Zero coverages and room temperature were used as initial conditions of the catalysts in this simulation. Because of relatively low exhaust gas flow rates and very low raw NO_x concentrations emitted from the considered Diesel engine (cf. $y^{in}_{NO_x}$ in Fig. 12b), a half-size NSRC (cf. Table 1) has been considered here. With this half-size NSRC, the average SV during the driving cycle was slightly more than 40 000 h^{-1}.

The smaller NSRC that is located first in the flow direction heats-up quite fast, while the larger SCR located downstream exhibits a delayed temperature response (cf. Fig. 12a). It can be seen that the NO_x conversion in the NSRC is getting slightly worse in the second and third cycles as the regeneration of the stored NO_x is not complete — cf. the increasing $y^{out,NSRC}_{NO_x}$ in Fig. 12b.

Calculated concentration profiles for the stored NO_x inside the NSRC are shown in Fig. 13a. The NO_x reduction front during the enrichment proceeds from the front part of the NSRC towards the outlet, so that the rear part is reduced less efficiently within the applied 3 s rich period. In the fourth cycle we can observe gradual stabilisation of the cyclic operation, indicating that the NO_x storage and reduction rates in the NSRC are approaching a stable balance. (Note that higher NO_x coverage slows down the NO_x storage and accelerates the regeneration, cf. Table 2.)

This evolution of the NO_x outlet concentrations is consistent with the increasing ammonia peaks during the regenerations — more NH_3 is produced with higher NO_x coverage, particularly in the rear part of the monolith [18,28]. An inverse trend is observed for the SCR efficiency: During the first EUDC cycle the SCR gives almost no NO_x conversion, because the initial ammonia coverage is zero and the SCR catalyst is not heated up properly, however, in the following EUDC cycles an additional NO_x reduction in the SCR can be seen, minimising the NO_x breakthrough from the NSRC (cf. Fig. 12b).

Two ammonia peaks are generated by the NSRC regenerations per each of the five EUDC cycles repeated in the simulation — the first one at lower temperature, and the second one at the high temperature corresponding to high engine load (cf. Fig. 12a). The

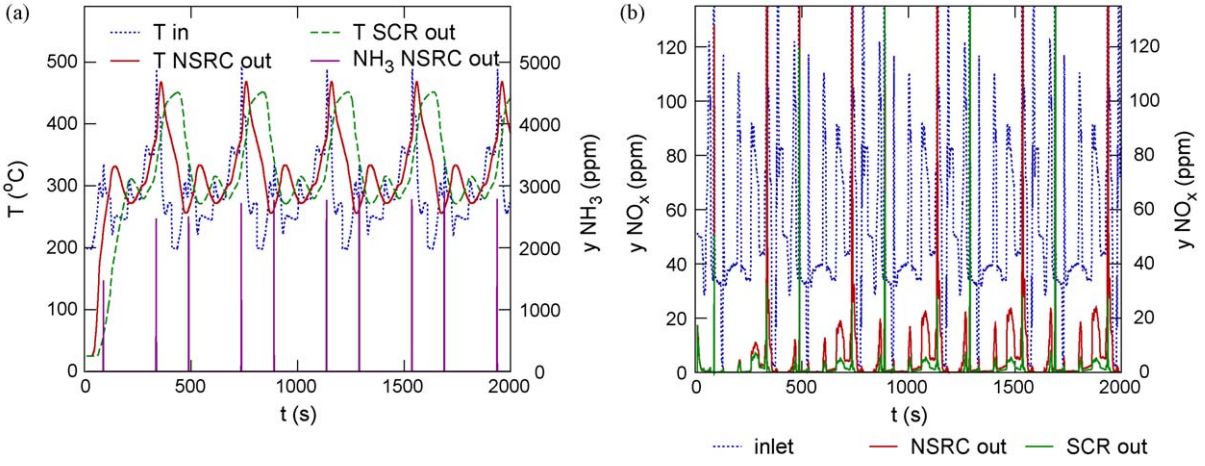

Fig. 12. Evolution of temperatures and concentrations of NH_3 (a) and NO_x (b) in the NSRC + SCR system during the 5× EUDC driving cycle. Each NSRC regeneration is accompanied by a NH_3 peak. The NO_x spikes during the NSRC regeneration going out of the depicted range are 300–600 ppm at maximum. Adiabatic half-size NSRC and full-size SCR in series (cf. Table 1), average SV in NSRC ≈40 000 h^{-1}.

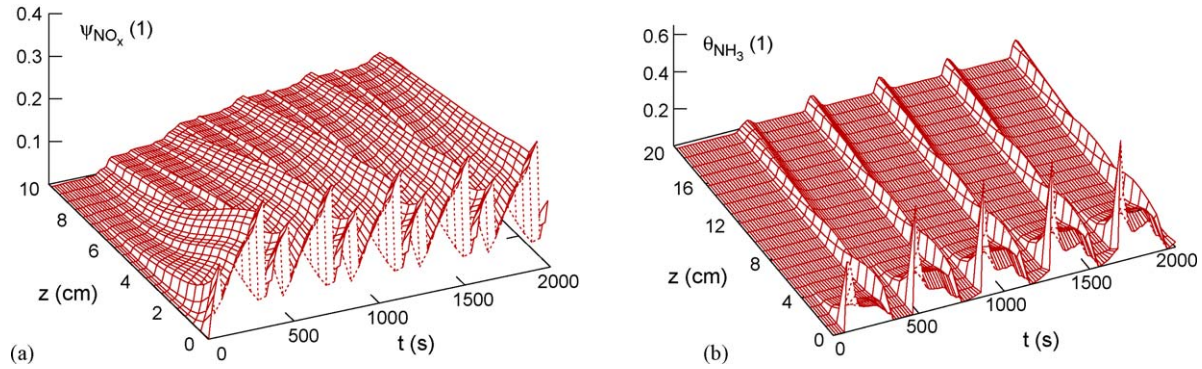

Fig. 13. Calculated spatio-temporal concentration profiles of the stored NO_x inside the NSRC monolith (a), and adsorbed NH_3 inside the SCR monolith (b), during the 5× EUDC driving cycle with combined NSRC + SCR system. Spatial coordinate $z = 0$ denotes inlet of the respective converter. Adiabatic half-size NSRC and full-size SCR in series (cf. Table 1), average SV in NSRC $\approx 40\,000\,h^{-1}$.

first NH_3 peak is adsorbed and utilised completely in the downstream SCR monolith, while the second NH_3 peak partly breaks through. Corresponding concentration profiles of the ammonia stored in the SCR are shown in Fig. 13b. Here the rapid adsorption of the first NH_3 peak at lower temperature is reflected by a steep increase of the NH_3 coverage in the front part of the reactor. The adsorbed NH_3 is then gradually removed by the SCR reaction with NO_x. The partial breakthrough of the second ammonia peak at the high temperature is indicated by a wave of increased local NH_3 coverage moving towards the SCR outlet. As already mentioned, this is due to a lower NH_3 adsorption capacity of the SCR catalyst at the high temperature.

The integral NO_x conversion over the 5× EUDC driving cycle depicted in Fig. 12 is 85.2% with the aged NSRC alone, and 96.9% for the combined NSRC + SCR system. The conversion just over the first EUDC cycle is 91.9% with the NSRC alone, and (coincidentally) again 96.9% for the combined NSRC + SCR system. The better conversion in the NSRC over the first cycle is caused by the fact that the simulation started with a perfectly regenerated catalyst (zero initial NO_x coverage). In the real operation of the exhaust gas aftertreatment system, a certain residual amount of the stored NO_x needs to be expected at the beginning.

In the final part of this section we will demonstrate that a location of the SCR farther behind the NSRC (similarly as it is in Fig. 2) can eliminate the SCR over-heating and loss of the NH_3 adsorption capacity. Furthermore, a shorter NSRC regeneration was examined in order to limit the ammonia production in the NSRC while keeping the NO_x conversions high. Alternative 5× EUDC cycle simulations were conducted with the following changes with respect to the original configuration: (i) A connecting pipe was considered between the NSRC and SCR monoliths (pipe length 1.0 m, steel, outer diameter 6.0 cm, inner diameter 5.7 cm, ambient temperature 20 °C, free convection of air outside). (ii) A shorter second regeneration in each EUDC was considered (2.5 s instead of the original 3.0 s). The results of these simulations are summarised in Fig. 14.

It can be seen that the connecting pipe significantly lowers the high temperature peak after the second regeneration, while the cooling effect at lower temperatures is less pronounced, which is consistent with the assumption of a constant ambient temperature. This elimination of the hot peak improves the NH_3 adsorption in the SCR and lowers its breakthrough, so that the overall ammonia yield is decreased from 14.5% to 5.0% (cf. Fig. 14), while the overall NO_x conversion remains approximately the same (96.9% and 96.2%, respectively).

The NH_3 emissions from the NSRC can be limited by shorter or less intensive NSRC regenerations. To demonstrate this effect, every second rich phase was shortened from 3.0 s to 2.5 s. As a consequence, both NH_3 yield and NO_x conversion in the NSRC decreased, by 8% and 4%, respectively (cf. Fig. 14b). The relatively

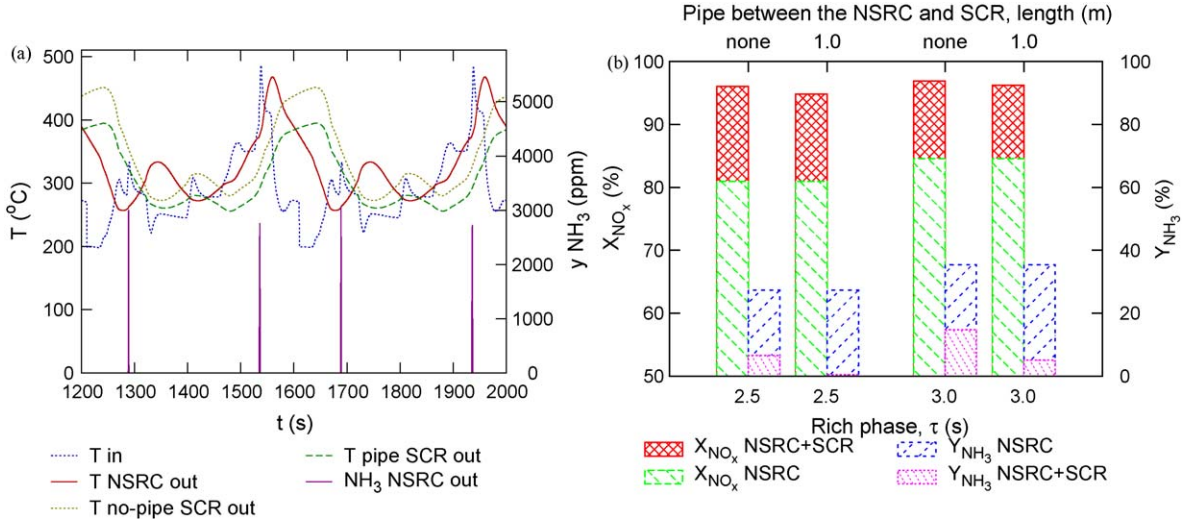

Fig. 14. (a) Evolution of temperatures in the combined system with and without a connecting pipe between the NSRC and SCR (the last two cycles from the 5× EUDC shown). (b) Effects of the connecting pipe and every second rich phase length on the integral NO_x conversions and NH_3 yields over the 5× EUDC driving cycle. Adiabatic half-size NSRC and full-size SCR in series (cf. Table 1), connecting pipe: length 1.0 m, steel, outer diameter 6.0 cm, inner diameter 5.7 cm, ambient temperature 20 °C.

large difference in the NO_x conversion and NH_3 yield for the 3.0 and 2.5 s enrichments confirms that the control of the rich phase is a key part of the NSRC operation. However, the overall NO_x conversion in the combined NSRC + SCR system decreased only by 1% as still enough ammonia was produced to enable the NH_3-SCR that compensated the NSRC conversion decrease. Because more NH_3 was consumed in the SCR, its overall NSRC + SCR yield was decreased to 6.6%. From these results it can be concluded that the shorter enrichments are more suitable in the studied case. With the longer rich phase more NH_3 and less NO_x is emitted from the NSRC, so that the ammonia is in excess and cannot be completely utilised in the SCR reactions.

If both the connecting pipe and the shorter regenerations are considered, the overall NO_x conversion decreases to 94.8% (i.e. 2% below the original level) but almost no NH_3 leaves the combined system during the studied driving cycle (the overall NH_3 yield is less than 0.5%, cf. Fig. 14b).

6. Conclusions

The combination of NSRC and SCR catalysts offers the potential to significantly increase the efficiency of NSRC-based exhaust gas aftertreatment systems. The presented results confirm this statement and reveal the potential of the system. Under most situations, the SCR catalyst is able to adsorb the NH_3 peaks generated in the NSRC during the regeneration and utilise it for further NO_x reduction. This synergy becomes more important with the aged NSRC where generally higher NH_3 yields in wider range of operating temperatures are observed in comparison with the fresh or de-greened NSRC, as discussed in the NSRC section of this paper.

The performance of the NSRC + SCR system was simulated with varying temperature and rich phase length, and their effects on NO_x conversions and NH_3 yields were discussed. The presented simulation results indicate that in the case of higher operating temperatures (that are beneficial for the NSRC regeneration), it is advantageous to locate the SCR reactor at a cooler place downstream in the exhaust gas line to prevent a loss of its NH_3 adsorption capacity.

The design and application of a combined exhaust gas aftertreatment system is a complex task involving engine management and different catalyst technologies. Simulation is an important element in design and optimisation of the system and its operating strategy. The models based on chemical and physical fundamentals are required because of the large variation in operating conditions. However, the complexity of the models must be kept at a reasonable level to avoid excessively long computations (large and stiff system) or too complicated evaluation of parameters during the calibration. For this purpose, properly designed global kinetics that incorporate important mechanisms of the reactions is a reasonable choice.

In this paper we have presented global kinetic models for the NSRC and SCR catalysts. The models consider explicitly the key surface-deposited species: the stored NO_x and O_2 in the NSRC, and the adsorbed NH_3 in the SCR. These species exhibit significant accumulation in the washcoat and their coverages determine to a large extent the local reaction rates as well as overall conversions. The interaction between mechanistic understanding and modelling of the relevant chemical and physical processes in the NSRC and SCR played a key role in the development of the combined NSRC + SCR system and enabled to bring this technology to series production [15].

Acknowledgements

The authors would like to thank Enrico Tronconi and Isabella Nova (Politecnico di Milano) for intensive and fruitful co-operation on NH_3-SCR experiments and modelling. Oscar Montoya is acknowledged for supporting us during the model validation phase.

References

[1] A. Güthenke, D. Chatterjee, M. Weibel, B. Krutzsch, P. Kočí, M. Marek, I. Nova, E. Tronconi, Current status of modelling lean exhaust gas aftertreatment catalysts, in: G.B. Marin (Ed.), Advances in Chemical Engineering 33: Automotive Emission Control, Elsevier, Amsterdam, 2007, pp. 103–211.
[2] Dieselnet http://www.dieselnet.com (2009).
[3] P. Forzatti, L. Lietti, E. Tronconi, Nitrogen oxides removal, in: I.T. Horvath (Ed.), Industrial Encyclopedia of Catalysis, Wiley, New York, 2002.
[4] R.H. Heck, R.J. Farrauto, S.T. Gulati, Catalytic Air Pollution Control, 2nd edition, John Wiley & Sons, New York, 2002.
[5] C. Enderle, G. Vent, M. Paule, F. Duvinage, SAE Tech. Paper 2008-01-1182 (2008).
[6] F. Birkhold, U. Meingast, P. Wassermann, O. Deutschmann, SAE Tech. Paper 2006-01-0643 (2006).
[7] N. Miyoshi, S. Matsumoto, K. Katoh, T. Tanaka, J. Harada, N. Takahara, SAE Tech. Paper 950809 (1995).
[8] W. Bögner, M. Krämer, B. Krutzsch, S. Pischinger, D. Voigtländer, G. Wenninger, F. Wirbeleit, M.S. Brogan, R.J. Brisley, D.E. Webster, Appl. Catal. B: Environ. 7 (1995) 153.
[9] N. Takahashi, H. Shinjoh, T. Iijima, T. Suzuki, K. Yamazaki, K. Yokota, H. Suzuki, N. Miyoshi, S. Matsumoto, T. Tanizawa, T. Tanaka, S. Tateishi, K. Kasahara, Catal. Today 27 (1996) 63.
[10] T. Kobayashi, T. Yamada, K. Kayano, SAE Tech. Paper 970745 (1997).
[11] W.S. Epling, L.E. Campbell, A. Yezerets, N.W. Currier, J.E. Parks, Catal. Rev. 46 (2004) 163.
[12] I. Grisstede, F. Rohr, S. Bremm, SAE Tech. Paper 2009-01-0632 (2009).
[13] B. Konrad, B. Krutzsch, D. Voigtländer, M. Weibel, Patent EP 957 242 B1 (1998). Corresponding Patent US 6,176,079 B1 (2001).
[14] J. Günther, B. Konrad, B. Krutzsch, A. Nolte, D. Voigtländer, M. Weibel, M. Weirich, G. Wenninger, Patent US 6,338,244 B1 (2002).
[15] M. Weibel, N. Waldbüßer, R. Wunsch, D. Chatterjee, B. Bandl-Konrad, B. Krutzsch, Top. Catal. 52 (2009) 1702–1708.
[16] T. Nakatsuji, M. Matsubara, J. Rouistenmki, N. Sato, H. Ohno, Appl. Catal. B: Environ. 77 (2007) 190–201.
[17] E.C. Corbos, M. Haneda, X. Courtois, P. Marecot, D. Duprez, H. Hamada, Appl. Catal. A: Gen. 365 (2009) 187–193.
[18] P. Kočí, F. Plát, J. Štěpánek, S. Bartova, M. Marek, M. Kubicek, V. Schmeißer, D. Chatterjee, M. Weibel, Catal. Today 147S (2009) S257–S264.
[19] D. Chatterjee, T. Burkhardt, B. Bandl-Konrad, T. Braun, E. Tronconi, I. Nova, C. Ciardelli, SAE Tech. Paper 2005-01-0965 (2005).
[20] D. Chatterjee, T. Burkhardt, M. Weibel, I. Nova, A. Grossale, E. Tronconi, SAE Tech. Paper 2007-01-1136 (2007).
[21] I. Nova, E. Tronconi, C. Ciardelli, D. Chatterjee, B. Bandl-Konrad, AIChE J. 52 (2006) 3222–3233.
[22] A. Grossale, I. Nova, E. Tronconi, D. Chatterjee, M. Weibel, J. Catal. 256 (2008) 312–322.
[23] D. Chatterjee, T. Burkhardt, T. Rappe, A. Güthenke, M. Weibel, SAE Tech. Paper 2008-01-0867 (2008).
[24] J.S. Choi, W.P. Partridge, W.S. Epling, N.W. Currier, T.M. Yonushonis, Catal. Today 114 (2006) 102.
[25] J.A. Pihl, J.E. Parks II, C.S. Daw, T.W. Root, SAE Tech. Paper 2006-01-3441 (2006).
[26] W.S. Epling, A. Yezerets, N.W. Currier, Appl. Catal. B: Environ. 74 (2007) 117.
[27] L. Cumaranatunge, S.S. Mulla, A. Yezerets, N.W. Currier, W.N. Delgass, F.H. Ribeiro, J. Catal. 246 (2007) 29.
[28] P. Kočí, F. Plát, J. Štěpánek, M. Kubíček, M. Marek, Catal. Today 137 (2008) 253–260.
[29] S.S. Mulla, S.S. Chaugule, A. Yezerets, N.W. Currier, W.N. Delgass, F.H. Ribeiro, Catal. Today 136 (2008) 136.
[30] L. Lietti, I. Nova, P. Forzatti, J. Catal. 257 (2008) 270.
[31] R.D. Clayton, M.P. Harold, V. Balakotaiah, Appl. Catal. B: Environ. 84 (2008) 616.
[32] A. Lindholm, N.W. Currier, J. Li, A. Yezerets, L. Olsson, J. Catal. 258 (2008) 273.
[33] J.P. Breen, R. Burch, C. Fontaine-Gautrelet, C. Hardacre, C. Rioche, Appl. Catal. B: Environ. 81 (2008) 150.
[34] P. Kočí, M. Kubíček, M. Marek, T. Maunula, M. Härkönen, Chem. Eng. J. 97 (2004) 131–139.
[35] Monolith research group http://www.vscht.cz/monolith (2009).
[36] J. Jirát, M. Kubíček, M. Marek, Catal. Today 53 (1999) 583–596.
[37] P. Kočí, M. Schejbal, J. Trdlička, T. Gregor, M. Kubíček, M. Marek, Catal. Today 119 (2007) 64–72.
[38] A. Güthenke, D. Chatterjee, M. Weibel, N. Waldbüßer, P. Kočí, M. Marek, M. Kubíček, Chem. Eng. Sci. 62 (2007) 5357.
[39] I. Nova, L. Lietti, L. Castoldi, E. Tronconi, P. Forzatti, J. Catal. 239 (2006) 244.
[40] M. Koebel, M. Elsener, G. Madia, Ind. Eng. Chem. Res. 40 (2001) 52–59.
[41] Y.H. Yeom, J. Henao, M.J. Li, W.M.H. Sachtler, E. Weitz, J. Catal. 231 (2005) 181–193.
[42] E. Tronconi, I. Nova, C. Ciardelli, D. Chatterjee, M. Weibel, J. Catal. 245 (2007) 1–10.
[43] A. Grossale, I. Nova, E. Tronconi, J. Catal. 265 (2009) 141–147.

[44] S. Malmberg, M. Votsmeier, J. Gieshoff, N. Sger, L. Mußmann, A. Schuler, A. Drochner, Top. Catal. 42 (2007) 33–36.
[45] L. Olsson, H. Sjövall, R.J. Blint, Appl. Catal. B: Environ. 81 (2008) 203.
[46] C. Ciardelli, I. Nova, E. Tronconi, B. Bandl-Konrad, D. Chatterjee, M. Weibel, B. Krutzsch, Appl. Catal. B: Environ. 70 (2007) 80–90.
[47] L. Lietti, I. Nova, E. Tronconi, P. Forzatti, M.A. Abraham, R.P. Hesketh, Reaction Engineering for Pollution Prevention, Elsevier, 2000, pp. 85–112.
[48] D. Chatterjee, T. Burkardt, M. Weibel, E. Tronconi, I. Nova, C. Ciardelli, SAE Tech. Paper 2006-01-0468 (2006).
[49] I. Nova, E. Tronconi, C. Ciardelli, D. Chatterjee, B. Bandl-Konrad, Catal. Today 114 (2006) 3–12.
[50] M. Devadas, O. Kröcher, M. Elsner, A. Wokaun, N. Söger, M. Pfeifer, Y. Demel, L. Mussmann, Appl. Catal. B: Environ. 67 (2006) 187–196.
[51] P. Forzatti, L. Lietti, Catal. Today, doi:10.1016/j.cattod.2008.11.023.